

Computational analysis of information-processing
properties in an echo-state network

19. ROČNÍK ČESKO-SLOVENSKEJ ŠVOČ V MATEMATIKE A INFORMATIKE

Autor: Miloslav Torda

Školiteľ: prof. Ing. Igor Farkaš, Dr.

2018

Abstract

Contents

1	Introduction	3
2	Theoretical background	5
2.1	General notion of artificial neural networks	5
2.1.1	Neural network as an approximation	6
2.1.2	Classes of neural networks	7
2.2	Echo state network	8
2.2.1	Architecture	8
2.2.2	Echo state property	9
2.2.3	Hyperparameters	9
2.2.4	Learning process	11
2.2.5	Short term memory capacity	11
2.2.6	Lyapunov characteristic exponent	12
2.2.7	Reservoir orthogonalization and orthonormalization	13
2.3	Information measures	14
2.3.1	Introduction to information theory	14
2.3.2	Limiting density of discrete points	16
2.3.3	Transfer entropy and active information storage	17
2.3.4	Transfer entropy and Granger causality	18
2.3.5	Estimation of transfer entropy and active information storage	19
2.3.6	Estimator parameter determination	22
2.3.7	Transfer entropy significance testing	24
3	Experiments	25
3.1	Experimental setup	25

3.1.1	Benchmark tasks	26
3.2	Information measures, performance and stability	28
3.2.1	MC task	29
3.2.2	NARMA task	29
3.2.3	M–G task	30
3.2.4	Lorenz task	31
3.2.5	Conclusion	31
3.3	Reservoir neuron signal embedding	33
3.3.1	MC task	34
3.3.2	NARMA task	34
3.3.3	M–G task	35
3.3.4	Lorenz task	35
3.3.5	Conclusion	36
3.4	Analysis of information transfer in the reservoir	36
3.4.1	MC task	38
3.4.2	NARMA task	40
3.4.3	M–G task	42
3.4.4	Lorenz task	44
3.4.5	Conclusion	47
4	Discussion	49
	Bibliography	51
A	Used software	54

Chapter 1

Introduction

With the development of deep learning, reservoir computing (RC) has lost momentum since introduction by Jaeger [14] regarding fast and simple neural network model. On the other hand recurrent neural networks (RNNs) are gaining a renewed interest as plausible models in neuroscience. For example Enel et al. [7] compare neural activity of prefrontal cortex of monkeys with a RC model trained to perform complex cognitive task and argue that similar network dynamics are manifested. Also in computer science, currently successful deep learning techniques make use of unsupervised RNNs (see [22]).

Considerable work has been done in regard to the stability of RC. Bertschinger and Natschläger [3] have shown that RNNs operating close to the transition from ordered to chaotic dynamics (critical point) support complex driven real-time computations. Similarly in biological neural networks it appears that cortical networks are optimized to function near the critical point (see [2]).

Some work has been done also from the information processing perspective of RNNs regarding stability regimes. Boedecker [4] has shown that in the echo state network model (ESN) that information measures, namely transfer entropy and active information storage, are maximized at the critical point. This thesis replicates and extends this work further by examining behaviour of ESN of two more driving input signals and takes a close look at information flow within the reservoir in various stability settings.

The thesis is organized as follows:

- in Section 2 we introduce the basic concept of an artificial neural network and the echo state network (ESN) architecture, together with some properties of ESNs, methods for setting up the parameters of the network, and methods to assess the

computational capabilities of the network model. Afterwards we continue with basic information theory and a more indepth overview of information measures used in this paper, namely transfer entropy and active information storage. We also cover some problems and solutions associated with the estimation of these measures.

- Section 3 presents conducted experiments and results. The first step was to explore the information-theoretical measures in the ESN reservoir around criticality. In the next step we explored the optimal embedding vectors of the reservoir neuron signals. In the final step we took a detailed look at information measures in ESN regarding various stability settings.
- The thesis concludes with summarizing the results from Section 3, and proposes possible explanations and continuations for further study.

Chapter 2

Theoretical background

2.1 General notion of artificial neural networks

Artificial neural networks are getting more and more attention over the last decades as advances in raw computational power make it possible to implement these computationally heavy algorithms as well as recent achievements in better than human performance on certain tasks. In the next paragraphs we provide basic theoretical concepts behind artificial neural networks.

Neural network model

Haykin [12] defines a neural network in the following way:

Definition 1 *A neural network is a massively parallel distributed processor made up of simple processing units, which has a natural property for storing experiential knowledge and making it available for use. It resembles the brain in two respects:*

- 1. Knowledge is acquired by the network from its environment through a learning process.*
- 2. Interneuron connection strengths, known as synaptic weights, are used to store acquired knowledge.*

The basic information-processing unit is called a *neuron*. In mathematical terms the neuron k of a system consisting of N neurons, can be written as a pair of equations:

$$u_k = \sum_{j=1}^m w_{kj}x_j \quad (2.1)$$

$$y_k = \varphi(u_k + b_k) \quad (2.2)$$

where x_1, x_2, \dots, x_m are the *input signals*, $w_{k1}, w_{k2}, \dots, w_{km}$ are *synaptic weights*, u_k is called *linear combiner output* due to the input signals, b_k is called *bias*, $\varphi(\cdot)$ is the *activation function*, and y_k is the output signal of the neuron.

There are two basic activation functions:

1. *Threshold function*

$$\varphi(v) = \begin{cases} 1 & \text{if } v \geq 0 \\ 0 & \text{if } v < 0 \end{cases} \quad (2.3)$$

2. *Sigmoid function*

- logistic function

$$\varphi(v) = \frac{1}{1 + e^{-av}} \quad (2.4)$$

- hyperbolic tangent function

$$\varphi(v) = \tanh(v). \quad (2.5)$$

2.1.1 Neural network as an approximation

One way to look at artificial neural networks is as a mapping

$$f : X \rightarrow Y$$

where X is the set of inputs and Y is the set of outputs. In the language of statistics we are dealing with nonparametric statistical inference. This view is strongly supported by an important theoretical result proved by Hornik [13], namely the universal approximation theorem.

Theorem 1 *Let*

$$\mathfrak{N}_k^{(n)}(\varphi) = \left\{ y : \mathbb{R}^k \rightarrow \mathbb{R} \mid y(x) = \sum_{i=1}^n \beta_i \varphi\left(\sum_{j=1}^m w_{ij}x_j - b_i\right) \right\}$$

denote a set of all functions implemented by a network with n hidden units and one output unit. If φ is continuous, bounded and nonconstant, then $\mathfrak{N}_k^{(n)}$ is dense in $C(X)$ for all compact subsets X of \mathbb{R}^k ($C(X)$ is the space of all continuous functions on X).

Here we can observe some similarities to the Stone-Weierstrass theorem (it implies that the set of all polynomials of X is dense in $C(X)$). The process of estimation of the synaptical weights w_{ij} for $i = 1, \dots, n$ and $j = 1, \dots, m$ is called *learning*.

2.1.2 Classes of neural networks

The neurons of a neural network can be organized into many different structures. Many have been already developed and successfully applied to different tasks. The structure is called *network architecture* and in general there are two fundamentally different classes of network architectures:

1. Feedforward networks

The structure of neurons is organized in layers. There is an *input layer*, *hidden layer* and *output layer*. The synaptical weights are only between neurons of two concurrent layers and only in one direction. In other words the output signals from one layer serve as input signals to the neurons in the second layer. We say that the network is *fully connected* if every unit in each layer of the network is connected to every unit in the next layer. Otherwise we say that the network is *partially connected*. In general there can be multiple hidden layers. Theorem 1 deals with a feedforward network with a single hidden layer. The standard learning algorithm for feedforward networks is called *backpropagation of error*. Basically it is a form of gradient based optimisation method.

2. Recurrent networks

A recurrent neural network that has at least one *feedback loop*. Feedback as is used in dynamical systems, that is when the output influences the input of an element of the system. In the setting of a neural network let us consider linear operators A and B , and an input-output relationship between two neurons

$$y_k(n) = A[x'_j(n)]$$

and

$$x'_j(n) = x_j(n) + B[y_k(n)].$$

Modifying these equations we get

$$y_k(n) = \frac{A}{1-AB}[x_j(n)].$$

We call the term $\frac{A}{1-AB}$ a *closed-loop operator* of the system, and AB the *open-loop operator*. Generally the existence of feedback loops in the neural network makes the process of learning very difficult.

2.2 Echo state network

Echo state networks (ESNs) belong to the class of recurrent neural networks. This type of architecture was first proposed by Jaeger [14]. In the next paragraphs we will provide the structure and some properties of an echo state network.

2.2.1 Architecture

The architecture consists of an input layer, a reservoir and an output layer. The reservoir is a fully connected recurrent hidden layer. The update equations are given by

$$\bar{\mathbf{x}}(t) = \tanh(\mathbf{W}^{\text{in}}[1; \mathbf{u}(t)] + \mathbf{W}\mathbf{x}(t-1)) \quad (2.6)$$

$$\mathbf{x}(t) = (1 - \alpha)\mathbf{x}(t-1) + \alpha\bar{\mathbf{x}}(t) \quad (2.7)$$

where $\mathbf{x}(t) \in \mathbb{R}^{N_x}$ is a vector of reservoir neuron activations and $\bar{\mathbf{x}}(t) \in \mathbb{R}^{N_x}$ is its update at time step t , $\tanh(\cdot)$ is the activation function, $\mathbf{W}^{\text{in}} \in \mathbb{R}^{N_x \times (1+N_u)}$ is the input weight matrix, $\mathbf{W} \in \mathbb{R}^{N_x \times N_x}$ is the recurrent weight matrix, and $\alpha \in (0, 1]$ is the leaking rate. The output is defined as

$$\mathbf{y}(t) = \mathbf{W}^{\text{out}}[1; \mathbf{u}(t); \mathbf{x}(t)] \quad (2.8)$$

where $\mathbf{y}(t) \in \mathbb{R}^{N_y}$ is network output and $\mathbf{W}^{\text{out}} \in \mathbb{R}^{N_y \times (1+N_u+N_x)}$ is the output weight matrix.

Lukoševičius [18] writes that the reservoir serves two functions:

1. as a high-dimensional nonlinear expansion, similarly to kernel methods, where input in input space is not linearly separable and by projecting in a higher dimensional space it may become linearly separable.
2. as a dynamical short-term memory.

2.2.2 Echo state property

Jaeger [14] defined the term *echo state property*, which is a necessary condition for the ESN to work in order to asymptotically wash out any information from initial conditions. The definition for a network with no output feedback is as follows:

Definition 2 *Assume that input is drawn from a compact input space U and network states lie in a compact set A . Assume that the network has no output feedback connections and let T be a network state update operator. Then, the network has echo states, if the network state $\mathbf{x}(n)$ is uniquely determined by any left-infinite input sequence $\bar{\mathbf{u}}^{-\infty}$. More precisely, this means that for every input sequence $\dots, \mathbf{u}(n-1), \mathbf{u}(n) \in U^{-\mathbb{N}}$, for all state sequences $\dots, \mathbf{x}(n-1), \mathbf{x}(n)$ and $\mathbf{x}'(n-1), \mathbf{x}'(n) \in A^{-\mathbb{N}}$, where $\mathbf{x}(i) = T(\mathbf{x}(i-1), \mathbf{u}(i))$ and $\mathbf{x}'(i) = T(\mathbf{x}'(i-1), \mathbf{u}(i))$, it holds that $\mathbf{x}(n) = \mathbf{x}'(n)$.*

2.2.3 Hyperparameters

The specific instance of an ESN is defined by a set of parameters, namely $(\mathbf{W}^{\text{in}}, \mathbf{W}, \alpha)$. In the next paragraphs we will outline the principles for choosing these parameters. We are going to follow the recommendations according to Lukoševičius [18].

1. *Reservoir matrix \mathbf{W}*
 - *Reservoir size* - the consensus is that the larger number of neurons in the reservoir the better, but on the other hand there is danger of over-parametrization and over-fitting. In general

$$T \geq 1 + N_x + N_u$$

where T is the dataset size, N_x is the number of neurons in the reservoir, and N_u is the input dimension.

- *Distribution of reservoir weights* - at the initialisation step of the algorithm the elements of the matrix \mathbf{W} are randomly generated and not manipulated afterwards. The weights are drawn independently from a uniform or normal distribution symmetrical around zero.
- *Spectral radius* - as stated in section 2.2.2 the existence of the echo state property in an ESN is essential for the network to work. Jaeger [14] states the network has no echo state when the spectral radius of the reservoir matrix is $|\lambda_{\max}(\mathbf{W})| > 1$, the admissible state set is $[-1, 1]^N$ and if the input set contains 0. Thus it is standard practice to scale the reservoir matrix \mathbf{W} so that $|\lambda_{\max}(\mathbf{W})| < 1$. The specific value $|\lambda_{\max}(\mathbf{W})|$ has to be determined experimentally in way that maximizes performance.

2. Input matrix \mathbf{W}^{in}

Similarly to the initialization of the reservoir matrix \mathbf{W} , the elements of input matrix \mathbf{W}^{in} are randomly selected either from uniform or normal symmetrical distribution.

3. Leaking rate α

Assume a dynamical system

$$\dot{\mathbf{x}} = -\mathbf{x} + \tanh(\mathbf{W}^{in}[1; \mathbf{u}] + \mathbf{W}\mathbf{x})$$

and using a discretization of the system

$$\dot{\mathbf{x}} \approx \frac{\mathbf{x}(t) - \mathbf{x}(t-1)}{\Delta t}$$

we get

$$\mathbf{x}(t) = (1 - \Delta t)\mathbf{x}(t-1) + \Delta t \tanh(\mathbf{W}^{in}[1; \mathbf{u}(t)] + \mathbf{W}\mathbf{x}(t-1)). \quad (2.9)$$

By comparing equations (2.7) and (2.9) we can regard the leaking rate parameter as the size of the discrete time step and scale accordingly. In practice this parameter has to be determined experimentally.

2.2.4 Learning process

As can be seen from previous sections there hasn't been any training involved yet. The only training is in finding the output layer weight matrix \mathbf{W}^{out} , precisely solving

$$\mathbf{Y}^{\text{target}} = \mathbf{W}^{\text{out}}\mathbf{X} \quad (2.10)$$

where $\mathbf{Y}^{\text{target}} \in \mathbb{R}^{N_y \times T}$, $\mathbf{X} \in \mathbb{R}^{(1+N_u+N_x) \times T}$ and T is the size of the training set. Lukoševičius [18] proposed to use regression with Tikhonov regularization

$$\mathbf{W}^{\text{out}} = \mathbf{Y}^{\text{target}}\mathbf{X}^{\text{T}}(\mathbf{X}\mathbf{X}^{\text{T}} + \beta\mathbf{I})^{-1} \quad (2.11)$$

where $\beta \in \mathbb{R}$ is the regularization parameter that has to be determined experimentally. When $\beta = 0$ we get

$$\mathbf{W}^{\text{out}} = \mathbf{Y}^{\text{target}}\mathbf{X}^+ \quad (2.12)$$

where $\mathbf{X}^+ = \mathbf{X}^{\text{T}}(\mathbf{X}\mathbf{X}^{\text{T}})^{-1}$ is the right Moore-Penrose inverse.

2.2.5 Short term memory capacity

As has been already stated, due to the feedback loops, echo state networks can be regarded as a dynamic short-term memory. Jaeger [15] defined a measure to quantify the reservoir ability to store and recall past input. It is called the short-term memory capacity:

Definition 3 *Let $\nu(n) \in U$ (where $-\infty < n < +\infty$ and $U \in \mathbb{R}$ is a compact interval) be a single-channel stationary input signal. Assume that we have a recurrent neural network, specified by its internal weight matrix \mathbf{W} , its input weight (column) vector \mathbf{w}^{in} and are suitable activation functions $\mathbf{f}, \mathbf{f}^{\text{out}}$. The network receives $\nu(n)$ at its input unit. For a given delay k and an output unit y_k with connection weight (row) vector $\mathbf{w}_k^{\text{out}}$ we consider the determination coefficient*

$$\begin{aligned} d[\mathbf{w}_k^{\text{out}}](\nu(n-k), y_k(n)) &= d\left(\nu(n-k), \mathbf{w}_k^{\text{out}} \begin{pmatrix} \nu(n) \\ \mathbf{x}(n) \end{pmatrix}\right) \\ &= \frac{\text{cov}^2(\nu(n-k), y_k(n))}{\sigma^2(\nu(n))\sigma^2(y_k(n))} \end{aligned} \quad (2.13)$$

where *cov* denotes covariance and σ^2 variance.

1. The k -delay short term memory capacity of the network is defined by

$$MC_k = \max_{\mathbf{w}_k^{out}} d[\mathbf{w}_k^{out}](\nu(n-k), y_k(n)). \quad (2.14)$$

2. The short term memory capacity of the network is

$$MC = \sum_{k=1}^{\infty} MC_k. \quad (2.15)$$

Jaeger [15] also proved a theoretical limit for the short-term memory capacity:

Proposition 1 *The memory capacity for recalling i.i.d input by a N -unit recurrent neural network with linear output units is bounded by N .*

2.2.6 Lyapunov characteristic exponent

The reservoir of an echo state network can be looked at as a discrete dynamical system and the performance of the whole network depends on its stability. A popular measure of the degree of the instability of a dynamical system is called *the maximum Lyapunov characteristic exponent*.

Definition 4 *Let*

$$\mathbf{x}(t+1) = \mathbf{f}(\mathbf{x}(t)) \quad (2.16)$$

be a discrete time dynamical system and

$$\mathbf{x}'(0) = \mathbf{x}(0) + \delta\mathbf{x}(0) \quad (2.17)$$

be the initial conditions a trajectory $\mathbf{x}'(t)$ obtained by an infinitesimal displacement from $\mathbf{x}(0)$ such that $\gamma_0 = \|\delta\mathbf{x}(0)\| \ll 1$. Then the maximum Lyapunov characteristic exponent is

$$\lambda = \lim_{t \rightarrow \infty} \frac{1}{t} \ln \left(\frac{\gamma_t}{\gamma_0} \right) < \infty \quad (2.18)$$

where $\gamma_t = \|\mathbf{x}'(t) - \mathbf{x}(t)\|$.

From the approximation

$$\gamma_t \sim \gamma_0 e^{\lambda t} \quad (2.19)$$

it can be seen that for $\lambda > 0$ the system is sensitive to initial conditions and therefore is chaotic. For $\lambda < 0$ the system is sub-critical. The value $\lambda \approx 0$ is when phase transition occurs and is often referred to as the edge of criticality or critical point.

For numerical computation of λ we implement a popular method according to Cencini et.al [6].

1. We start with an infinitesimal perturbation γ_0 and evolve the system one time step ahead, thus getting a normalized tangent vector $\mathbf{w}(1) = \frac{\mathbf{x}'(1) - \mathbf{x}(1)}{\gamma_0}$ and setting $\alpha(1) = \|\mathbf{w}(1)\|$.
2. Next we rescale $\mathbf{w}(1)$ to $\frac{\mathbf{w}(1)}{\|\mathbf{w}(1)\|}$ and evolve the system one step ahead again. We repeat this process and store the amplitudes $\alpha(t) = \|\mathbf{w}(t)\|$.
3. The maximum Lyapunov exponent is obtained as:

$$\lambda = \lim_{t \rightarrow \infty} \frac{1}{t} \sum_{i=1}^t \ln(\alpha(i)). \quad (2.20)$$

In the echo state network setting we set the infinitesimal perturbation to every neuron unit individually and compute λ_i of the i -th perturbed for every $i = 1, \dots, N$ of the N unit reservoir. The final estimated is computed as average $\lambda = \langle \lambda_i \rangle$.

2.2.7 Reservoir orthogonalization and orthonormalization

We have already mentioned reservoir matrix scaling according to the desired spectral radius. Another ways to scale the reservoir matrix is in relation to orthogonality. More precisely to satisfy the condition $\mathbf{W}^\top \mathbf{W} = \mathbf{I}$. Farkaš et. al. [8] proposed a gradient based orthogonalization and orthonormalization methods and have shown that the theoretical limits in the memory capacity task, proved by Jaeger [15], can be achieved via these methods.

The update formula in case of the orthogonalization method is

$$\Delta \mathbf{w}_i = -\eta \frac{4}{\|\mathbf{w}_i\|} (\mathbf{I} - \tilde{\mathbf{w}}_i \tilde{\mathbf{w}}_i^\top) (\tilde{\mathbf{W}} \tilde{\mathbf{W}}^\top) \tilde{\mathbf{w}}_i \quad (2.21)$$

where η is the learning rate and $\tilde{\mathbf{W}}$ denotes matrix \mathbf{W} with normalized columns using Frobenius norm.

The update formula for the orthonormalization method is

$$\Delta \mathbf{w}_i = -\eta 4 (\mathbf{W} \mathbf{W}^\top \mathbf{W} - \mathbf{W}). \quad (2.22)$$

2.3 Information measures

2.3.1 Introduction to information theory

In order to get an insight into transfer entropy and active information storage we have to define some key information theoretic concepts. We will follow the definitions according to MacKay [19]. At first we define the Shannon information content and entropy of a discrete random variable X with the set of outcomes \mathcal{A}_X .

Definition 5 *Shannon information content of an outcome x is defined to be*

$$h(x) = \log_2 \frac{1}{P(x)}. \quad (2.23)$$

The units are called bits.

Definition 6 *The entropy of a random variable X is defined to be the average Shannon information content of an outcome:*

$$\begin{aligned} H(X) &= \sum_{x \in \mathcal{A}_X} P(x) \log \frac{1}{P(x)} \quad \text{for } P(x) \neq 0 \\ &= 0 \quad \text{for } P(x) = 0 \end{aligned} \quad (2.24)$$

since $\lim_{\theta \rightarrow 0^+} \theta \log \frac{1}{\theta} = 0$.

In later text we are going to use another important information theoretic concept, namely the relative entropy or Kullback-Leibler divergence.

Definition 7 *The relative entropy or Kullback-Leibler divergence between two probability distributions $P(x)$ and $Q(x)$ that are defined over the same \mathcal{A}_X is*

$$D_{KL}(P||Q) = \sum_{x \in \mathcal{A}_X} P(x) \frac{P(x)}{Q(x)}. \quad (2.25)$$

From the Gibb's inequality follows one important property of relative entropy. That is

$$D_{KL}(P||Q) \geq 0$$

with equality only if $P = Q$.

Next we need to define conditional entropy.

Definition 8 *The conditional entropy of X given $y = b_k$ is the entropy of the probability distribution $P(x | y = b_k)$.*

$$H(X | y = b_k) = \sum_{x \in \mathcal{A}_X} P(x | y = b_k) \log \frac{1}{P(x | y = b_k)} \quad (2.26)$$

Definition 9 *The conditional entropy of X given Y is average, over y , of the conditional entropy of X given y .*

$$\begin{aligned} H(X | Y) &= \sum_{y \in \mathcal{A}_Y} P(y) \left[\sum_{x \in \mathcal{A}_X} P(x | y) \log \frac{1}{P(x | y)} \right] \\ &= \sum_{x \in \mathcal{A}_X, y \in \mathcal{A}_Y} P(x, y) \log \frac{1}{P(x | y)}. \end{aligned} \quad (2.27)$$

The interpretation of conditional transfer entropy is that it measures the average uncertainty that remains about X when Y is known.

Now we can define mutual information and conditional mutual information.

Definition 10 *The mutual information between X and Y is*

$$I(X; Y) = H(X) - H(X | Y). \quad (2.28)$$

Mutual information measures the reduction of uncertainty about X that results from learning the value of y .

Definition 11 *The conditional mutual information between X and Y given $z = c_k$ is the mutual information between the random variables X and Y in the joint ensemble $P(x, y | z = c_k)$,*

$$I(X; Y | z = c_k) = H(X | z = c_k) - H(X | Y, z = c_k). \quad (2.29)$$

Definition 12 *The conditional mutual information between X and Y given $z = c_k$ is the mutual information between the random variables X and Y in the joint ensemble $P(x, y | z = c_k)$,*

$$I(X; Y | z = c_k) = H(X | z = c_k) - H(X | Y, z = c_k). \quad (2.30)$$

Definition 13 *The conditional mutual information between X and Y given Z is the average over z of the conditional mutual information from Definition 12.*

$$I(X; Y | Z) = H(X | Z) - H(X | Y, Z). \quad (2.31)$$

Entropy and all other measures based on entropy we have just introduced are defined for a discrete set of probabilities. Shannon [24] analogously defined the entropy of a continuous distribution with the density distribution function $p(x)$ as

$$H(X) = \int_{-\infty}^{\infty} p(x) \log \frac{1}{p(x)} dx. \quad (2.32)$$

This quantity is sometimes called *differential entropy* although this is not a measure of uncertainty of the random variable X as Shannon intended it to be.

Similarly, from the identity

$$I(X; Y) = \sum_{x \in \mathcal{A}_X, y \in \mathcal{A}_Y} P(x, y) \log \frac{P(x, y)}{P(x)P(y)} \quad (2.33)$$

we can define mutual information between two continuous random variables as:

$$I(X; Y) = \int_{-\infty}^{\infty} \int_{-\infty}^{\infty} p(x, y) \log \frac{p(x, y)}{p(x)p(y)} dx dy. \quad (2.34)$$

2.3.2 Limiting density of discrete points

As already noted in the previous section, Shannon's formulation of entropy for continuous variables is not an information measure. First it lacks many properties of discrete entropy and second it is not a result of any proper derivation. Nevertheless differential entropy has many theoretical applications.

Jaynes [16] proposed a different approach to defining entropy of a continuous variable. Let $x_i, i = 1, \dots, n$ be discrete points such that

$$\lim_{n \rightarrow \infty} \frac{1}{n} (\text{number of points in } a < x < b) = \int_a^b m(x) dx \quad (2.35)$$

exists. Then the differences $(x_{i+1} - x_i)$ in the neighbourhood of any particular value of x will tend to zero so that

$$\lim_{n \rightarrow \infty} n(x_{i+1} - x_i) = m(x_i)^{-1}. \quad (2.36)$$

The discrete probability $P(x_i)$ from Definition 6 will transform to

$$P(x_i) = p(x_i)(x_{i+1} - x_i). \quad (2.37)$$

Equivalently from equation (2.36)

$$P(x_i) \rightarrow p(x_i) \frac{1}{nm(x_i)}. \quad (2.38)$$

Plugging (2.37) and (2.38) into the definition of Shannon entropy (definition 6) we get

$$H(X) \rightarrow - \int p(x) \log \left[\frac{p(x)}{nm(x)} \right] dx. \quad (2.39)$$

Following this reasoning, Jaynes defined the continuous information measure as:

$$\bar{H}(X) = \lim_{n \rightarrow \infty} [H(X) - \log(n)] = - \int p(x) \log \left[\frac{p(x)}{m(x)} \right] dx. \quad (2.40)$$

2.3.3 Transfer entropy and active information storage

Let $x(t)$ and $y(t)$ be the realizations of two processes $X(t)$ and $Y(t)$. Paluš [20] proposed, as an approach to measure the directional information rate, to measure conditional mutual information $I(y(t); x(t + \tau) | x(t))$. It is the average amount of information contained in the process $Y(t)$ about the process $X(t)$ in its future τ time units ahead conditioned on $X(t)$, as opposed to the mutual information $I(y(t); x(t + \tau))$ which can contain information about $X(t + \tau)$ in $X(t)$. Similarly Shreiber in [23] defines mutual information rate of two Markov processes $\{I\}$ and $\{J\}$ of order k and l by measuring the deviation from independence given by the Markov property $p(i_{t+1} | i_t^{(k)}) = p(i_{t+1} | i_t^{(k)}, j_t^{(l)})$ using conditional Kullback-Leibler divergence in the following form

$$\begin{aligned} D_{\text{KL}}(P(I_{t+1} | I_t^{(k)}, J_t^{(l)}) || P(I_{t+1} | I_t^{(k)})) &= \\ &= \sum p(i_{t+1}, i_t^{(k)}, j_t^{(l)}) \log \frac{p(i_{t+1} | i_t^{(k)}, j_t^{(l)})}{p(i_{t+1} | i_t^{(k)})}. \end{aligned}$$

These ideas inspired the current definition of transfer entropy.

Definition 14 *Let X_t and Y_t be two processes. The transfer entropy from the source Y with the history length k to the target X with history length l is*

$$T_{Y \rightarrow X}^{(k,l)} = I(X_t ; \mathbf{Y}_{t-1}^{(l)} | \mathbf{X}_{t-1}^{(k)}) \quad (2.41)$$

where

$$\begin{aligned} \mathbf{X}_{t-1}^{(k)} &= (X_{t-1}, X_{t-1-\tau_k}, X_{t-1-2\tau_k}, \dots, X_{t-1-(k-1)\tau_k}) \\ \mathbf{Y}_{t-1}^{(l)} &= (Y_{t-1}, Y_{t-1-\tau_l}, Y_{t-1-2\tau_l}, \dots, Y_{t-1-(l-1)\tau_l}). \end{aligned}$$

From the identity for conditional mutual information

$$I(X; Y | Z) = H(X) - I(X; Z) - H(X | Y, Z)$$

it follows that transfer entropy can be expressed as

$$T_{Y \rightarrow X}^{(k,l)} = H(X_t) - I(X_t | \mathbf{X}_{t-1}^{(k)}) + H(X_t | \mathbf{Y}_{t-1}^{(l)}, \mathbf{X}_{t-1}^{(k)}).$$

The second term on the right in the expression above has a special significance for us.

Definition 15 *The active information storage of the process X with history length k is*

$$A_X^{(k)} = I(\mathbf{X}_{t-1}^{(k)}; X_t) = H(X_t) - H(X_t | \mathbf{X}_{t-1}^{(k)}). \quad (2.42)$$

The active information storage measures the amount of information in the past state of $\mathbf{X}_t^{(k)}$ of X about its next value X_t .

2.3.4 Transfer entropy and Granger causality

Transfer entropy is closely related to another concept of dependency, namely Granger causality. This relationship provides a different interpretation of the concept of transfer entropy. Let us take a closer look at it.

We take the definition of Granger causality from [5]

Definition 16 *Using the notation from Definition 14. Let $F(x_t | \mathbf{x}_{t-1}^{(k)}, \mathbf{y}_{t-1}^{(l)})$ be the distribution function of the target variable X_t conditional on $\mathbf{X}_{t-1}^{(k)}, \mathbf{Y}_{t-1}^{(l)}$ and $F(x_t | \mathbf{x}_{t-1}^{(k)})$ be the distribution function of X_t conditional on its own past. Then variable Y is said to Granger-cause variable X if*

$$F(x_t | \mathbf{x}_{t-1}^{(k)}, \mathbf{y}_{t-1}^{(l)}) \neq F(x_t | \mathbf{x}_{t-1}^{(k)}). \quad (2.43)$$

Now, consider two linear regression models

$$X_t = A_1 X_{t-1} + \dots + A_k X_{t-k} + B_1 Y_{t-1} + \dots + B_l Y_{t-l} + \epsilon_t \quad (2.44)$$

$$X_t = A'_1 X_{t-1} + \dots + A'_k X_{t-k} + \epsilon'_t \quad (2.45)$$

with model parameters of the models A_i, A'_i, B'_j . Geweke in [9] defined the measure of Granger causality from Y to X in the following way,

$$F_{Y \rightarrow X}^{(k,l)} = \log(|\text{var}(\epsilon'_t)| / |\text{var}(\epsilon_t)|) \quad (2.46)$$

where $|\cdot|$ denotes the determinant. We can observe that this is actually log-likelihood ratio test under the null hypothesis

$$H_0 : B_1 = \dots = B_l = 0 \quad (2.47)$$

when the residuals of the both models are gaussian.

From the definitions of Transfer entropy (definition 14) and Granger causality (definition 16) it can be seen that both transfer entropy and Granger causality are measures of predictive causality. The similarity is even closer when we consider the joint process X_t, Y_t as multivariate gaussian. Barnett et. al. [1] proved that under these conditions Granger causality and transfer entropy are equivalent up to factor 2 i.e.

$$F_{Y \rightarrow X}^{(k,l)} = 2T_{Y \rightarrow X}^{(k,l)}. \quad (2.48)$$

2.3.5 Estimation of transfer entropy and active information storage

Estimation of information measures is still an open problem. Currently there are few available classes of estimators that one can choose from, based on the properties of the observed data. Transfer entropy is no exception and the best estimator given some specific criteria is yet to be determined. An overview of transfer entropy estimators can be found in [5] or [25].

We are going to focus on one specific estimator of the class of estimators based on k -nearest neighbour search. We chose this estimation method because they are currently considered data efficient and accurate nonparametric estimation techniques for continuous random variables.

Kozachenko-Leonenko Shannon entropy estimator

We are going to put the basic idea of behind Kozachenko-Leonenko differential entropy estimator as was presented in [17].

Let X be a continuous random variable, $f(x)$ be its density and its differential entropy as defined in (9). Specifically

$$H(X) = \int_{-\infty}^{\infty} f(x) \log \frac{1}{f(x)} dx. \quad (2.49)$$

Then the Monte-Carlo estimate of $H(X)$ is

$$\widehat{H}(X) = \frac{1}{N} \sum_{i=1}^N \log \frac{1}{f(x_i)}. \quad (2.50)$$

Since we don't know $f(x_i)$ it has to be substituted by an estimate $\widehat{f}(x_i)$ which we are going to find using k -nearest neighbours of x_i .

Let $P_k(\epsilon)$ be the probability distribution of the distance between x_i and its k th nearest neighbour. Then $P_k(\epsilon)d\epsilon$ is the probability that there is one point in the r distance from x_i where $r \in \left[\frac{\epsilon}{2}; \frac{\epsilon}{2} + \frac{d\epsilon}{2} \right]$, $k-1$ points are at distances less than r and $N-k-1$ points are at distances greater than k th nearest neighbour. Using multinomial distribution formula we get

$$P_k(\epsilon)d\epsilon = \frac{(N-1)!}{1!(k-1)!(N-k-1)!} \left(\frac{dp_i(\epsilon)}{d\epsilon} d\epsilon \right) (p_i(\epsilon))^{k-1} (1-p_i(\epsilon))^{N-k-1} \quad (2.51)$$

where $p_i(\epsilon)$ is the probability mass of ϵ ball centered at x_i , that is

$$p_i(\epsilon) = \int_{\|\xi - x_i\| < \frac{\epsilon}{2}} f(\xi) d\xi. \quad (2.52)$$

It follows from (2.51) and (2.52) that the expectation value $\log p_i(\epsilon)$ is given by

$$\begin{aligned} E(\log p_i(\epsilon)) &= \int_0^\infty \log p_i(\epsilon) P_k(\epsilon) d\epsilon \\ &= \psi(k) - \psi(N) \end{aligned} \quad (2.53)$$

where $\psi(x)$ is the digamma function.

If we assume that $f(x)$ is constant in the entire ϵ ball we can approximate $p_i(\epsilon)$ by

$$p_i(\epsilon) \approx c_d \epsilon^d f(x_i), \quad (2.54)$$

where d is the dimension of x and c_d is the volume of the d -dimensional unit ball. For the maximum norm $c_d = 1$.

Finally taking the logarithm and expectation of (2.54), and combining it with (2.53) and (2.50) we get Kozachenko-Leonenko entropy estimator

$$\widehat{H}(X) = -\psi(k) + \psi(N) + \log c_d + \frac{d}{N} \sum_{i=1}^N \log \epsilon(i), \quad (2.55)$$

where $\epsilon(i)$ is twice the distance from x_i to its k th nearest neighbour.

Kraskov–Stögbauer–Grassberger mutual information estimator

Kraskov, Stögbauer and Grassberger [17] came up with a method of using Kozachenko-Leoneko entropy estimator to estimate mutual information. Using the identity

$$I(X, Y) = H(X) + H(Y) - H(X, Y) \quad (2.56)$$

we are going to obtain an estimator $\widehat{I}(X, Y)$.

First we directly apply Kozachenko-Leonenko entropy estimator to joint random variable $Z = (X, Y)$ with maximum norm and we get

$$\widehat{H}(X, Y) = -\psi(k) + \psi(N) + \frac{d_X + d_Y}{N} \sum_{i=1}^N \log \epsilon(i) \quad (2.57)$$

where $\epsilon(i)$ is the $\frac{\epsilon}{2}$ from z_i to its k th nearest neighbour and $d_Z = d_X + d_Y$.

For the estimate of $H(X)$ we take the distance $\epsilon(i)$ from (2.57) as an approximation of $[n_x(i) + 1]$ st nearest neighbour of x_i , where $n_x(i)$ is the number of points in within $\|x_j - x_i\| < \frac{\epsilon}{2}$, and we get

$$\widehat{H}(X) = -\frac{1}{N} \sum_{i=1}^N \psi(n_x(i) + 1) + \psi(N) + \frac{d_X}{N} \sum_{i=1}^N \log \epsilon(i). \quad (2.58)$$

Analogously for the marginal space Y we get

$$\widehat{H}(Y) = -\frac{1}{N} \sum_{i=1}^N \psi(n_y(i) + 1) + \psi(N) + \frac{d_Y}{N} \sum_{i=1}^N \log \epsilon(i). \quad (2.59)$$

Combining (2.56), (2.57), (2.58) and (2.59) we get the Kraskov, Stögbauer and Grassberger (KSG) estimator

$$I^{(1)}(X, Y) = \psi(k) - \langle \psi(n_x + 1) + \psi(n_y + 1) \rangle + \psi(N) \quad (2.60)$$

where $\langle \dots \rangle = \frac{1}{N} \sum_{i=1}^N (\dots)$.

Estimating transfer entropy and active information storage.

Since active information storage of a process is defined in definition 15 as mutual information between its current and past state, it follows from (2.60) that the active information estimator is written as

$$\widehat{A}_X^{(k)} = \psi(k) + \psi(N) - \left\langle \psi(n_{\mathbf{x}_{t-1}^{(k)}} + 1) + \psi(n_{x_t} + 1) \right\rangle. \quad (2.61)$$

As for an estimate of transfer entropy Gomez-Herrero et al. [10] generalized the idea of Kraskov et. al. [17]. Let $V = (V_1, \dots, V_m)$ be a random m -dimensional vector. Then the entropy combination is defined as

$$C(V_{\mathcal{L}_1}, \dots, V_{\mathcal{L}_p}) = \sum_{i=1}^p s_i H(V_{\mathcal{L}_i}) - H(V) \quad (2.62)$$

where $\forall i \in [1, p] : \mathcal{L}_i \subset [1, m]$ and $s_i \in \{-1, 1\}$ such that $\sum_{i=1}^p s_i \chi_{\mathcal{L}_i} = \chi_{[1, m]}$ where χ_S is characteristic function of S and the entropy combination estimator is given by

$$\widehat{C}(V_{\mathcal{L}_1}, \dots, V_{\mathcal{L}_p}) = F(k) - \sum_{i=1}^p s_i \langle F(k_i(j)) \rangle \quad (2.63)$$

where $F(k) = \psi(k) - \psi(N)$ and $k_i(j) = n_{V_{\mathcal{L}_i}}(j) + 1$ for $j = 1, \dots, N$ as formulated in section 2.3.5.

For example, from equation (2.56) it can be seen that mutual information is an entropy combination. Similarly from the one of the expressions for conditional mutual information

$$I(X; Y | Z) = H(X, Z) + H(Y, Z) - H(Z) - H(X, Y, Z) \quad (2.64)$$

it follows that $I(X; Y | Z)$ is also an entropy combination and combining (2.63) and (2.64) we get the KSG estimator for conditional mutual information

$$\widehat{I}(X; Y | Z) = \psi(k) - \langle \psi(n_{xz} + 1) + \psi(n_{yz} + 1) - \psi(n_z + 1) \rangle. \quad (2.65)$$

Finally directly from definition 14 we get the KSG transfer entropy estimator

$$\widehat{T}_{Y \rightarrow X}^{(k, l)} = \psi(k) - \left\langle \psi(n_{x_t, \mathbf{x}_{t-1}^k} + 1) + \psi(n_{y_{t-1}^l, \mathbf{x}_{t-1}^k} + 1) - \psi(n_{\mathbf{x}_{t-1}^k} + 1) \right\rangle. \quad (2.66)$$

2.3.6 Estimator parameter determination

The KSG estimator belongs to a class of nonparametric estimation methods. Nevertheless, since it is based on k -nearest neighbour search, k in the nearest neighbour algorithm is one of the parameters we have to choose. This parameter has to be empirically determined. Kraskov et al. [17] suggest $k > 1$ but not too large because of the increase of systematic errors. Generally they propose to use k from 2 to 4. Bossomaier et al. [5] writes that for $k \geq 4$ the estimator is robust and Wibral [25] writes that $k = 4$ has been determined as a good choice for ECoG data.

Another problem is to determine the embedding vector as defined in definition 14. For example, in case of transfer entropy we would like as much of information that is contained in the target process about its own past to condition out. If we do not do this, the measured information transfer might be due to self prediction of the target process and not due to dependance of the source and target processes. The method for finding an optimal value for the embedding vector is also called state space reconstruction.

There are multiple methods to determine the state space vectors. One way is to set the pair of parameters (m, τ) such that it maximizes the active information storage. Wibral et al. [25] propose to optimize the embedding parameters using the Ragwitz–Kantz criterion.

Ragwitz and Kantz [21] proposed a method to extract a Markov process of order $m > 1$ from observed scalar time series using locally constant predictors. In the following paragraphs we will briefly describe this method.

Let $\mathbf{s}_n = (s_n, s_{n-\tau}, \dots, s_{n-(m-1)\tau})$ be time delay embedding vector such that $s_{n+1} = g(\mathbf{s}_n)$ exists. Then the locally constant predictor for the unobserved s_{n+1} is

$$\widehat{s}_{n+1} = \frac{1}{|\mathcal{U}_n|} \sum_{\mathbf{s}_k \in \mathcal{U}_n} s_{k+1} \quad (2.67)$$

i.e . the mean of the immediate futures of the ϵ -neighbours of \vec{s}_n where

$$\mathcal{U}_n = \{\mathbf{s}_k : \|\mathbf{s}_k - \mathbf{s}_n\| \leq \epsilon\}.$$

Ragwitz and Kantz in [21] argue that locally constant predictor is a predictor based on Markov transition probability assumption

$$p(s_{n+1} | s_n, s_{n-\tau}, \dots, s_{n-(m-1)\tau}) = p(s_{n+1} | s_n, s_{n-\tau}, \dots, s_{n-(m-1)\tau}).$$

To get the transition the probabilities $p(s_{n+1} | \mathbf{s}_n)$, a locally constant approximation is used in the form $p(s_{k+1} | \mathbf{s}_k) \approx \widehat{p}(s_{n+1} | \mathbf{s}_n) \forall \mathbf{s}_k \in \mathcal{U}_n$. The justification of a locally constant predictor follows then from the idea that if we use the mean square error of predictions $e^2 = \sum_{i=1}^N (s_{i+1} - \widehat{s}_{i+1})^2$ then the best estimator of s_{n+1} is

$$\widehat{s}_{n+1} = \int_{\vec{s}_k \in \mathcal{U}_n} s_{k+1} p(s_{k+1} | \mathbf{s}_n) d\mathbf{s}_{k+1} \quad (2.68)$$

Thus we take those time delay embedding vector parameters as optimal which minimize the locally constant prediction error i.e.

$$(m, \tau) = \arg \min_{m \in \mathbb{Z}, \tau \in \mathbb{Z}} \left\| \vec{s} - \widehat{\vec{s}} \right\|. \quad (2.69)$$

2.3.7 Transfer entropy significance testing

One of the problems that plague all transfer entropy estimators is bias. Either systematic errors or statistical errors are both the properties of estimators that have to be dealt with. If we observe a non-zero value of transfer entropy it can be due to bias or variance and the transfer entropy estimator (2.66) is no exception. Since KSG method is non-parametric one of the suggested statistical testing options is to use a permutation test [25] [5].

We are going to test the null hypothesis that there is no relationship between the source and target variables. First we have to come with surrogate source variable under to assumption that the null hypothesis is true. One way to do it is to by permuting $\mathbf{y}_{t-1}^{(l)}$ in the joint probability space $\{x_t, \mathbf{x}_{t-1}^{(k)}, \mathbf{y}_{t-1}^{(l)}\}$ thus destroying any predictive dependence of Y to X , and computing $T_{Y_{\text{sur}} \rightarrow X}$ of the surrogate source variable Y_{sur} . Repeating this procedure multiple times we can compute one-sided p -value of the test by the following equation:

$$P(T_{Y_{\text{sur}} \rightarrow X} \geq T_{Y \rightarrow X}) = \sum_{Y_{\text{sur}}: T_{Y_{\text{sur}} \rightarrow X} \geq T_{Y \rightarrow X}} P(Y_{\text{sur}}). \quad (2.70)$$

If the $p < 0.05$ we reject the null hypothesis at the 5% significance level.

Chapter 3

Experiments

Our aim was to explore the information flow within the ESN reservoir and its relationship to specified task performance. For this reason a specific ESN model had to be chosen. This meant fixing the hyperparameters of the model. At first we wanted to extend the work done by Boedecker et al. [4].

3.1 Experimental setup

For comparability reasons and consistence of results we choose the same ESN model and also two benchmark tasks used by Boedecker et. al. [4]. The benchmark tasks we used is memory capacity task, and one-step ahead prediction of one stochastic and two deterministic processes.

ESN setup

We used ESNs with $N = 100$ reservoir units. A single input neuron and Q output neurons depending on the task. Concretely 120 output neurons for the memory capacity task and 1 output neuron for the prediction tasks. We didn't use a bias unit in the input and output layers, nor direct input-output connections. The leaking rate in (2.7) was set to $\alpha = 0$. The input weight matrix was initialized from uniform distribution $\mathcal{U}(-0.1; 0.1)$. The elements of the reservoir matrix \mathbf{W} were drawn from normal distribution $\mathcal{N}(0; 0.5)$. Concerning the learning process, we set $\beta = 0$ in the Tikhonov regularization in expression (2.11), effectively getting direct pseudoinverse computation of the readout matrix \mathbf{W}^{out} . We discarded the first 100 samples of the reservoir neuron

activations in order to get the network running and to get rid of the transients, and 1000 samples of the reservoir neuron activations along with desired outputs were used to set the readout weights. Next 2000 samples from the network output were used to test the networks performance.

3.1.1 Benchmark tasks

In our experiments we used four standard benchmark tasks that are used by the reservoir computing community.

1. Memory capacity (MC)

In order to measure the networks ability to recall past input, a sequence of independent identically distributed real numbers drawn from uniform distribution on the closed interval $[-1; 1]$ was used as the driving signal.

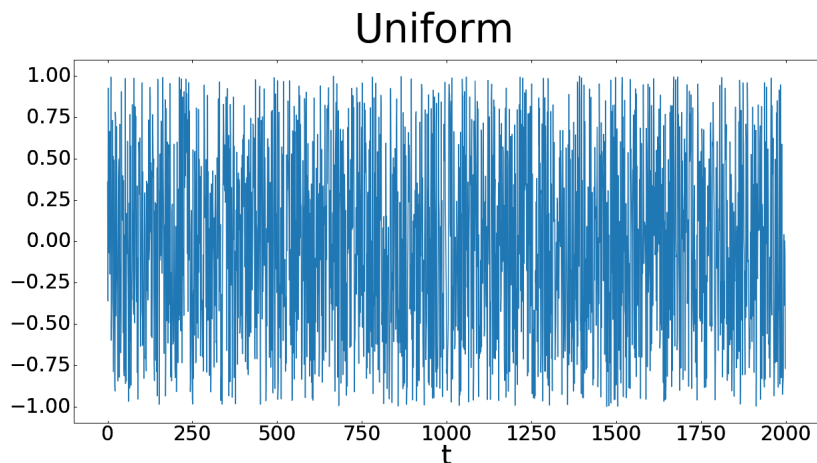


Figure 3.1: Input used in memory capacity task

2. NARMA

We used 30-th order NARMA time series for one time step ahead prediction. The NARMA model was given by the following formula:

$$u(t+1) = 0.2u(t) + 0.004u(t) \sum_{i=0}^{29} u(t-i) + 1.5q(t-29)q(t) + 0.001 \quad (3.1)$$

where $\forall t : q(t) \sim \mathcal{U}(0; 0.5)$.

3. Mackey-Glass system (M-G)

NARMA

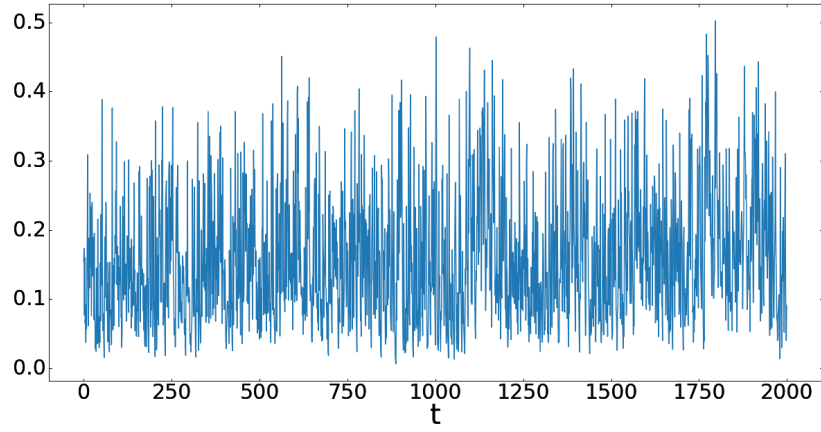


Figure 3.2: Input used in NARMA prediction task.

Another standard benchmark task we used is the one time step ahead prediction of the Mackey-Glass system. The system is given by time-delay differential equation

$$\frac{du}{dt} = 0.2 \frac{u_{17}}{1 + (u_{17})^{10}} - 0.1u \quad (3.2)$$

where u_{17} is the value of u at time $t - 17$.

M-G

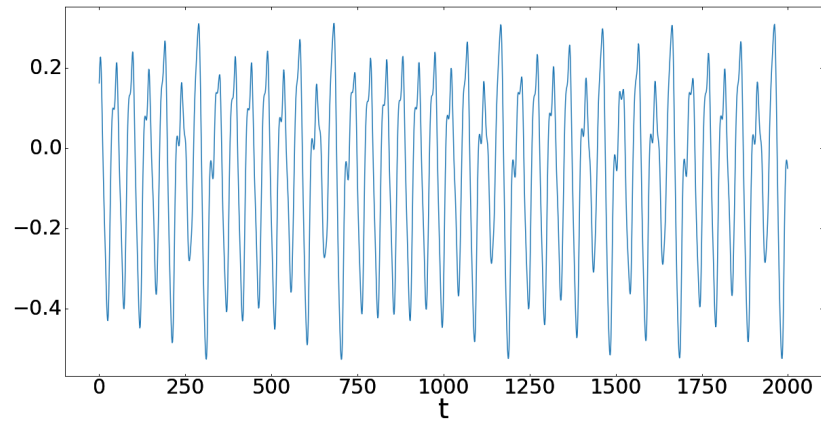


Figure 3.3: Input used in M-G prediction task.

4. Lorenz system

The last task was the one step ahead prediction of the x-coordinate of the Lorenz

system given by the following ordinary differential equations:

$$\frac{dx}{dt} = 10(y - x) \quad (3.3)$$

$$\frac{dy}{dt} = x(28 - z) - y \quad (3.4)$$

$$\frac{dz}{dt} = xy - \frac{8}{3}z. \quad (3.5)$$

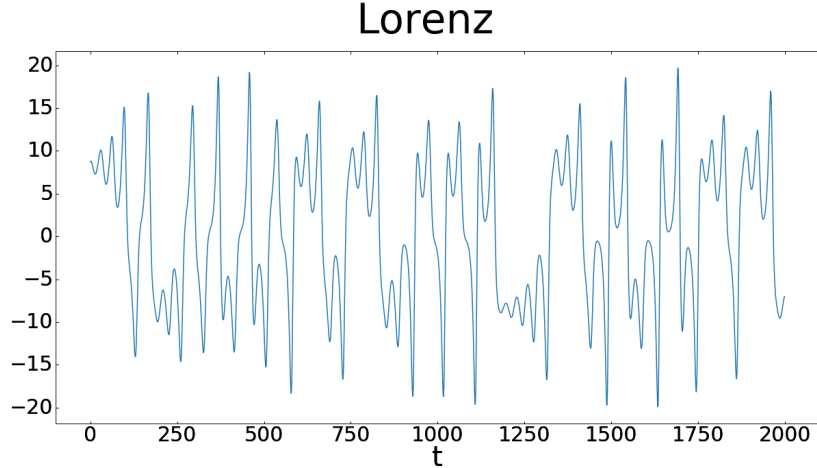


Figure 3.4: Input used in Lorenz prediction task.

Regarding the assessment of performance, for measuring the memory capacity task performance we used measures introduced in section 2.2.5 and in the cases of prediction tasks we used the normalized root mean square error computed as:

$$\text{NRMSE} = \sqrt{\frac{\langle (\hat{y}(t) - y(t))^2 \rangle_t}{\langle (y(t) - \langle y(t) \rangle_t)^2 \rangle_t}} \quad (3.6)$$

where $\hat{y}(t)$ denotes the predicted value of the process, $y(t)$ is the true value of the process and $\langle \cdot \rangle_t$ denotes the time-average.

3.2 Information measures, performance and stability

In order to explore the relationship between transfer entropy, active information storage and task performance we followed the idea of Boedecker [4] and computed average TE and AIS within the ESN reservoir for different stability modes. To assess the stability of reservoir we computed the maximum Lyapunov exponent introduced in section 2.2.6.

Since the maximum Lyapunov exponent can be manipulated only indirectly, we varied the variance σ of the distribution from which the elements of the reservoir matrix were drawn. To get a wide enough spectrum of stability instances we increased σ in such a way that $\log \sigma \in [-1.5; -0.25]$ in 26 steps. For every value of σ (step) we created 5 instances of reservoir matrices. Altogether 130 instances of reservoir matrices and for every such matrix we measured λ , its performance (MC/NRMSE), TE and AIS.

Concerning the setting of the TE and AIS estimators parameters, ideally we would determine them using Ragwitz-Kantz criterion introduced in section 2.3.6 but estimating optimal signal embedding for every neuron for every instance would be computationally demanding. Thus we set the target signal embedding in the TE computation and the signal embedding in AIS computation to $k = 2$ and $\tau_k = 1$, the source signal embedding in the TE computation to $l = 1$ and $\tau_l = 1$. We didn't change these settings in the course of simulations. In the same manner we set the number of nearest neighbour in the k-NN search to 4.

Since the KGS estimator has some inherent systematic error, for TE and AIS close to zero the $\widehat{\text{TE}}$ and $\widehat{\text{AIS}}$ estimates can be negative. From the definition of TE and AIS as special cases of Kullbeck–Leibler divergence, the values can be only non-negative. Therefore we have set all the negative values of TE and AIS in the experiments to zero since the purpose of the experiments was not to test whether there is some information transfer but to compare changes of information transfer in various settings.

3.2.1 MC task

The results in case of MC task are presented in Figure 3.5. The performance (MC) in this task peaks just before the phase transition from the stable regime to unstable regime. Similarly the information measures peak around the critical point $\lambda \approx 0$. MC, TE and AIS sharply drop to minimal values in the unstable mode ($\lambda > 0$). With decreasing λ in negative range, MC raises and unexpectedly TE falls steadily. AIS does not seem to change accordingly to the changes in TE and MC.

3.2.2 NARMA task

In case of the NARMA task the results are shown in Figure 3.6. The behavior of information measures and performance (NRMSE) is similar to the MC task. The

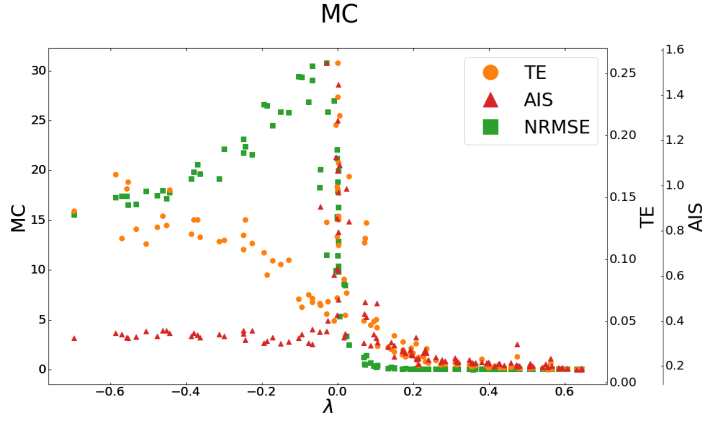


Figure 3.5: Average values of TE and AIS within the reservoir, and memory capacity in relation to the maximum Lyapunov exponent λ in the MC task. Every datum represents one instance of the reservoir matrix.

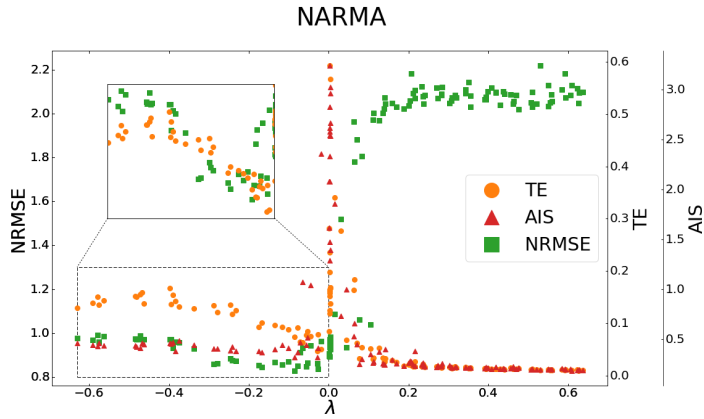


Figure 3.6: Average values of TE and AIS within the reservoir, and NRMSE in relation to the maximum Lyapunov exponent λ in the NARMA prediction task. Every datum represents one instance of the reservoir matrix.

performance peaks close to the phase transition ($\lambda \approx 0$), as well as TE and AIS, and falls sharply after the phase transition into the the unstable regime. Similarly to the MC task, the performance raises with increasing λ (NRMSE decreases) and also TE in the negative range. AIS doesn't seem to change accordingly.

3.2.3 M–G task

The behavior of information measures and performance in case of M–G task, shown in Figure 3.7, is quite different from previous tasks. First, the performance does not peak close to the phase transition, but rather in the more stable region ($\lambda \ll 0$) and second TE doesn't seem to change in relation to the performance as in the MC and NARMA

tasks. On the other hand information measures peak at criticality as in previous cases and fall sharply in the unstable region but AIS stays high for $\lambda > 0$.

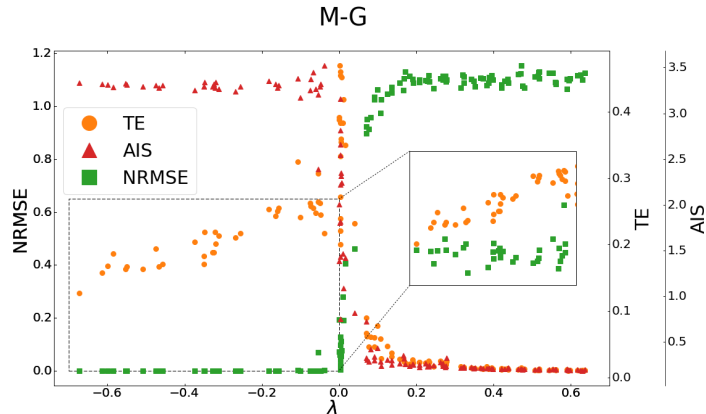


Figure 3.7: Average values of TE and AIS within the reservoir, and NRMSE in relation to the maximum Lyapunov exponent λ in the M–G prediction task. Every datum represents one instance of the reservoir matrix.

3.2.4 Lorenz task

The results from Lorenz task (Figure 3.8) resemble those from the M–G task in that the performance peaks in stable regime far from the critical point. TE and AIS also peak further from the critical point than in previous cases. The decrease of performance and information measures from the stable to unstable regime is more gradual than in previous cases indicating that our ESN model is less sensitive to the stability of the reservoir in case of Lorenz driving signal. There seems to be a relationship between TE and performance similar to the MC and NARMA in the stable mode.

3.2.5 Conclusion

From the observed results it seems that there is an unexpected relationship between the information measures and performance for λ in stable region. To look at this relationship we computed various correlation coefficients between corresponding information measure and the performance. As the transition from the stable to the unstable mode is gradual and task dependent, we looked at the instances for which λ is in stable mode, and such that it maximizes the Pearson correlation coefficient. Thus we gradually decreased the size of the interval beginning with $\lambda = 0$ and for each interval com-

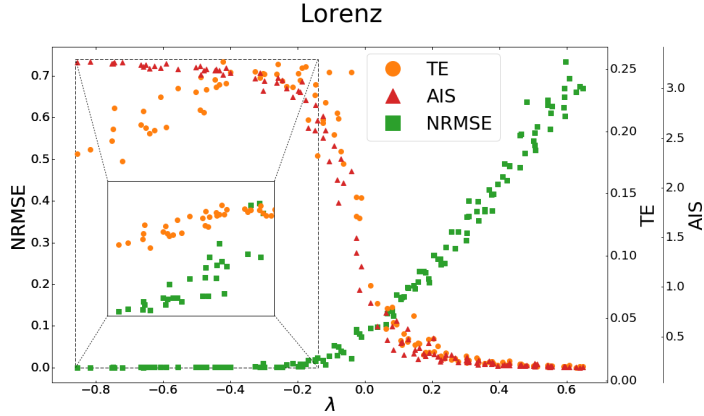


Figure 3.8: Average values of TE and AIS within the reservoir, and NRMSE in relation to the maximum Lyapunov exponent λ in the Lorenz prediction task. Every datum represents one instance of the reservoir matrix.

puted correlation coefficients. The results for maximal obtained Pearson correlation coefficients are presented in Table 3.1 for TE and Table 3.2 for AIS.

We want to emphasize that the use of the correlation coefficients in such a way is not correct. First the data we compute the correlations do not satisfy the assumptions necessary for statistical testing, and second the idea of looking for maximal correlations by search is questionable. Nevertheless we think it is a good way to explore for potential relationships within the stable region.

In case of TE, our explorations imply that there seems to be negative relationship between information flow and task performance at least for MC, NARMA and Lorenz tasks. That means the higher the performance the lower the overall information flow within the reservoir layer.

	MC		NARMA		M-G		Lorenz	
	$\lambda \in [-0.6, -0.0064)$		$\lambda \in [-0.6, -0.0017)$		$\lambda \in [-0.6, -0.0013)$		$\lambda \in [-0.9, -0.0233)$	
	Coeff.	p-value	Coeff.	p-value	Coeff.	p-value	Coeff.	p-value
Pearson	-0.920	1.9e-11	0.657	1.0e-05	0.706	9.3e-07	0.664	4.6e-05
Spearman	-0.897	6.6e-13	0.657	1.0e-05	0.240	0.17	0.779	2.4e-07
Kendall	-0.743	8.3e-09	0.444	1.0e-04	0.159	0.17	0.587	3.5e-06

Table 3.1: Values of correlation coefficients between TE and performance (MC or NRMSE depending on task) in stable regimes.

In case of AIS, the selfpredictability of the units in the reservoir seems to depend

on the task. For MC task there seems to be a negative relationship between AIS and performance, no relationship in NARMA and M-G tasks, and positive dependence in Lorenz task (note that higher performance means lower NRMSE in NARMA, M-G and Lorenz tasks, and higher MC in MC task). As if the network benefits more from the selfpredictability of each neuron than from information exchange between different units in the Lorenz task.

	MC		NARMA		M-G		Lorenz	
	$\lambda \in [-0.6, -0.0064)$		$\lambda \in [-0.6, -0.0017)$		$\lambda \in [-0.6, -0.0013)$		$\lambda \in [-0.9, -0.0233)$	
	Coeff.	p-value	Coeff.	p-value	Coeff.	p-value	Coeff.	p-value
Pearson correlation	-0.737	3.4e-06	0.01	0.954	-0.920	2.8e-16	-0.911	1.2e-12
Spearman correlation	-0.708	1.2e-05	0.452	0.005	0.051	0.763	-0.866	3.2e-10
Kendall correlation	-0.513	6.9e-05	0.3	0.009	0.038	0.734	-0.690	4.9e-08

Table 3.2: Values of correlation coefficients between AIS and performance (MC or NRMSE depending on task) in stable regimes.

Altogether the results indicate a surprising inverse relationship between TE and performance. To get a more precise answer to this hypothesis it is necessary to design the experiments more thoroughly.

3.3 Reservoir neuron signal embedding

In the next step we wanted to get a closer look at information measures at different stability settings but to achieve this, the values of KSG estimators parameters had to be chosen. As already mentioned in section 3.2, ideally we would determine the embedding vector and the time delay for every single neuron signal and use it in the TE and AIS estimation. This approach would computationally very demanding and the whole reservoir information measure estimation would be overparameterized. Thus we simplified this task and set the TE and AIS parameters to one value for every neuron in single reservoir.

To find this value we used the Ragwitz-Kantz criterion (section 2.3.6) to determine the embedding vectors for every neuron in 100 instances of reservoir matrices for every task and every scaling. Then the most frequent parameter observation in a specific task and scaling was taken as the optimal value in subsequent TE and AIS computations.

The search space in the Ragwitz-Kantz method was $k = 1, \dots, 6$ for the the embedding vector length and $\tau = 1, \dots, 6$ for the time delay.

The ESNs were initialized according to section 3.1. and subsequently the reservoir matrix was scaled in order to get a specific spectral radius (section 2.2.3) according to desired stability properties i.e. *unscaled* for unstable, $\rho = 0.6$ for stable and $\rho = 0.95$ close to criticality. We also added two more scalings of the reservoir matrix according to orthogonality/orthonormality introduced in section 2.2.7. We used the spectral radius scaling $\rho = 0.95$ and then ran 30 iterations of the OG method (eq. 2.21) with the learning rate $\eta = 0.03$. We did the same procedure with the ON method (eq. 2.22), except that the learning rate was set to $\eta = 0.07 * (0.9)^t$, $t = 0, \dots, 30$. Altogether we got 5 different scalings.

3.3.1 MC task

The results for the MC task are presented in Figure 3.9. The embedding length and delay exploration have single maxima for all scalings. The maxima seem insensitive to scalings of the reservoir matrix. Also the most frequent choices of embedding vectors are for the largest length allowed in the exploration, except for the scaling $\rho = 0.6$. Due to the stochastic nature of the driving signal in the MC task it seems that the single neuron signals can not be approximated by a Markov process and thus $k \rightarrow \infty$. Or the maximal allowed length in the exploration was to low.

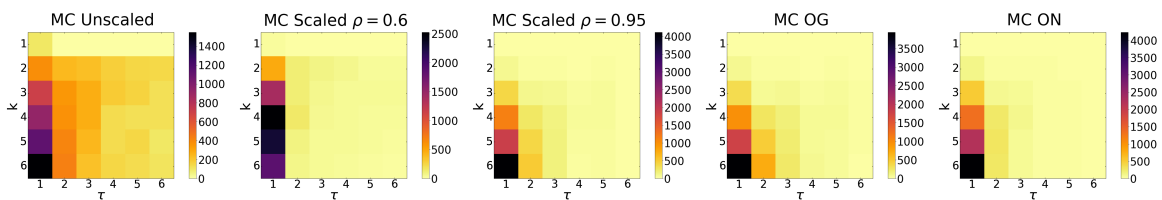


Figure 3.9: (k, τ) pairs for various scalings of the reservoir in MC task. Each cell denotes the number of occurrences when the locally constant predictor with the corresponding parameter pair minimized the prediction error in a single neuron signal.

3.3.2 NARMA task

In the case of NARMA task the results, shown in Figure 3.10, are almost identical to the result of the MC task. The maxima for every scaling are the same as in the

case of MC task. These similarities can be regarded as an indication that the neuron activation signals in the MC and NARMA tasks have some identical properties. For example the order of the underlying Markov process.

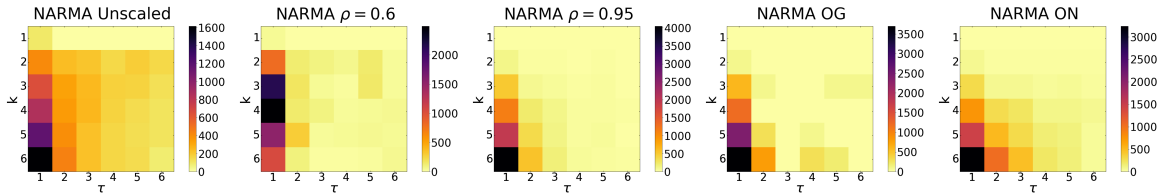


Figure 3.10: (k, τ) pairs for various scalings of the reservoir in NARMA task. Each cell denotes the number of occurrences when the locally constant predictor with the corresponding parameter pair minimized the prediction error in the single neuron signal.

3.3.3 M–G task

The results of the M–G task exploration are presented in Figure 3.11. In this case there are also single maxima but for the scaled instances there is a possibility of a second node for $\tau > 6$. The scalings of the reservoir matrix have a noticeable influence on the embedding vector choice, very different from the MC and NARMA tasks. This also implies that the scaled neuron signals for this task could be approximated by a Markov process of order 2.

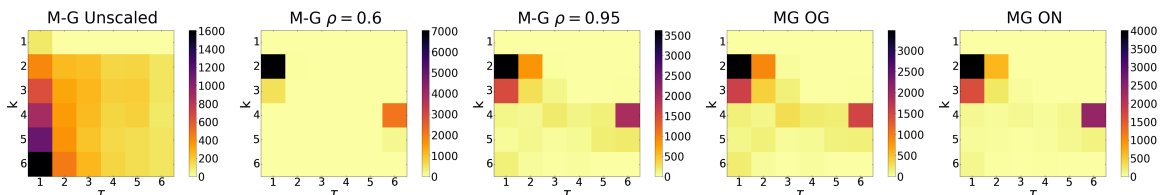


Figure 3.11: (k, τ) pairs for various scalings of the reservoir in M–G task. Each cell denotes the number of occurrences when the locally constant predictor with the corresponding parameter pair minimized the prediction error in the single neuron signal.

3.3.4 Lorenz task

The results for the Lorenz task (Figure 3.12) are similar to the M–G task in that they have singular maxima nodes and the length of the most frequent embedding vector is 2. The difference is in delay τ and that the distribution of winning (k, τ) pairs is more

spread than in previous cases. The higher delay τ could be explained by a small Δt time step when the training and validation dataset was created.

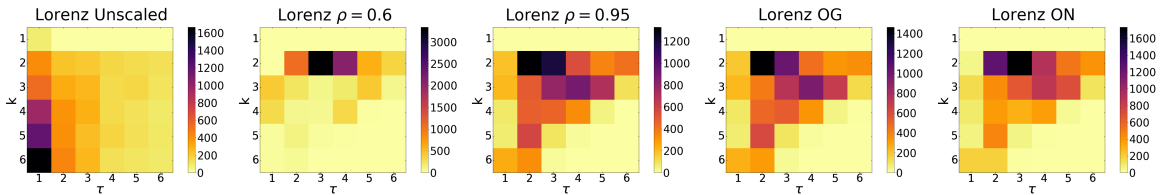


Figure 3.12: (k, τ) pairs for various scalings of the reservoir in Lorenz task. Each cell denotes the number of occurrences when the locally constant predictor with the corresponding parameter pair minimized the prediction error in the single neuron signal.

3.3.5 Conclusion

As a side product of the search for optimal values of the KSG estimators parameters which are presented in Table 3.3, we did get an insight into the complexity of reservoir neuron activation signals. If we consider the order of an underlying Markov process as a measure of how complex an observed time series is then the reservoir activations in the MC and NARMA tasks have the same complexity, and the same goes for M-G and Lorenz tasks. This was expected since the former are driven by a stochastic signal and the latter by a deterministic signal.

Task \ Scaling	MC		NARMA		M-G		Lorenz	
	k	τ	k	τ	k	τ	k	τ
init	6	1	6	1	6	1	6	1
$\rho = 0.6$	4	1	4	1	2	1	2	3
$\rho = 0.95$	6	1	6	1	2	1	2	2
OG	6	1	6	1	2	1	2	2
ON	6	1	6	1	2	1	2	3

Table 3.3: Most frequent (k, τ) pairs for each task and scaling.

3.4 Analysis of information transfer in the reservoir

In the final step we wanted to have a closer look at the behaviour of the reservoir in different settings (introduced in section 3.1) regarding the information transfer. We

generated one instance of the input weight vector \mathbf{w}^{in} and one instances of the recurrent weight matrix \mathbf{W} defined in section 3.1), and used them in all subsequent scalings and tasks. In the computations of the information measures in every task and scaling, we used the most frequent observations of the pair (k, τ) listed in table 3.3 as parameters of the target variable in the TE estimator and as global parameters in the AIS estimator. The source variable parameters in the TE estimator were set to $(1, 1)$, as we wanted to observe only how the most recent past of the source unit influences the target unit.

Similarly to section 3.2 we dealt with the problem of systematic error and negative value of TE and AIS estimations. In this case we chose to implement the permutation test for TE introduced in section 2.3.7. For every $\widehat{TE}_{Y \rightarrow X}$ we computed p -value from 100 surrogate source variables Y_{sur} generated from the corresponding source variable Y . We set $\widehat{TE}_{Y \rightarrow X} = 0$ if $p > 0.05$. Negative AIS values were set to zero in same manner as in section 3.2.

In order to quantify not only the global changes of information transfer due to scalings but also the changes in distribution of TE (when we consider the values of TE as a random variable), we computed relative entropy (Kullbeck–Liebler divergence) of TE, because the relative entropy is according to section 2.3.2 a more suitable measure of disorder (uncertainty) in a system when considering a continuous random variable then differential entropy. For the probability distribution $m(x)$ in eq. 2.40, we chose the uniform distribution as it maximizes the differential entropy when no prior knowledge about the distribution is available ¹. We choose the support of the uniform distribution to be the closed interval $[0; \max \text{TE}]$ where $\max \text{TE}$ is the maximum observed value of TE in a specific task and scaling. The estimator of the relative entropy takes the following form:

$$\begin{aligned} \left| \overline{H} \left(\text{TE}_{\text{RES}}^{(k,l)} \right) \right| &= \widehat{D}_{\text{KL}} \left(\text{TE}_{\text{RES}}^{(k,l)} \parallel \mathcal{U} \left(0; \max \left\{ \text{TE}_{\text{RES}}^{(k,l)} \right\} \right) \right) \\ &= \ln \left(\max \left\{ \text{TE}_{\text{RES}}^{(k,l)} \right\} \right) - \widehat{H}_{\text{KL}} \left(\text{TE}_{\text{RES}}^{(k,l)} \right) \end{aligned} \quad (3.7)$$

where $\ln(\max \text{TE}_{\text{RES}}^{(k,l)})$ is the exact differential entropy of the uniform distribution with the support in $[0; \max \text{TE}_{\text{RES}}^{(k,l)}]$, $\widehat{H}_{\text{KL}}(\cdot)$ is the Kozachenko-Leonenko entropy estima-

¹It can be proved that the uniform distribution has the maximum differential entropy among all continuous distributions supported in the closed interval $[a, b]$. The proof follows from the non-negativity property of Kullbeck-Liebler divergence

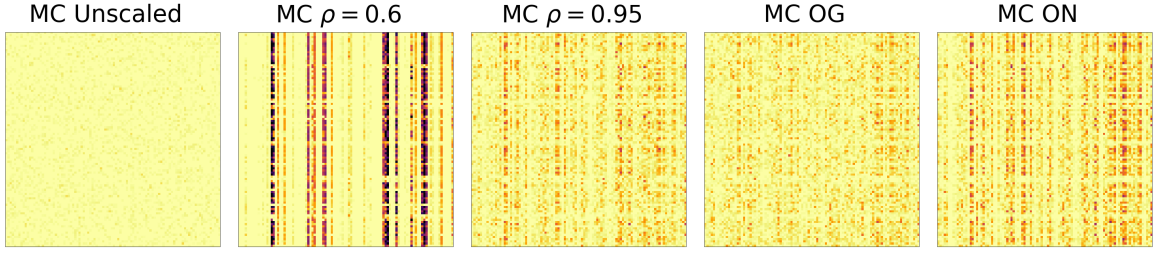


Figure 3.13: The matrices ($N \times N$) of TE values in the reservoir for different scalings in MC task. Rows of the matrix denote source units and columns denote target units. Dark color represents high values, light color represents low values.

tor(introduced in section 2.3.5) and $TE_{RES}^{(l,k)}$ is the distribution of the estimates of transfer entropies in the reservoir.

3.4.1 MC task

The visualisation of TE in reservoir for 5 different scalings in case of MC task is presented in figure 3.13. There is a noticeable change in the amount of TE by the transition from unscaled to scaled reservoir. Unscaled represents unstable regime, and scalings to spectral radius $\rho = 0.6$ and $\rho = 0.95$ represent stable regime and criticality respectively. Corresponding Lyapunov exponents λ values are listed in table ???. In case of $\rho = 0.6$ there are a few target neurons that have high values of TE (dark columns). The transition to criticality leads to the performance rising and global value of TE decreasing, as observed in section 3.2.1. Concerning the OG and ON scalings there is an improved performance in case of OG and similar decrease of TE.

Figure 3.14 plots histograms of distribution of TE in corresponding reservoir scaling. We can observe the most visible changes from unscaled, to $\rho = 0.6$ and to $\rho = 0.95$. The quantification of the level of disorder of TE within the maximum value in every scaling is represented in table ?? by the relative entropy of TE. The unscaled case has the lowest value of relative entropy which means its distribution is closest to the uniform distribution. We can interpret this result that the unscaled case has the highest level of disorder of TE among all scalings. With the transition to $\rho = 0.6$ the level of disorder decreases and further decreases towards the criticality scaling. An interesting observation is that the OG scaling has the highest performance lowest TE and highest relative entropy of TE among the scalings $\rho = 0.6$, $\rho = 0.95$, OG and ON.

Figure 3.15 provides the visualisation of the changes in AIS due to scaling for every

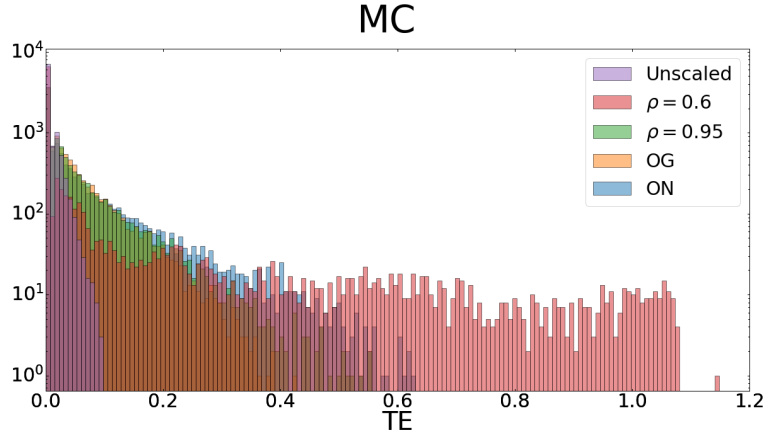


Figure 3.14: Histograms of TE distribution changes due to reservoir scaling in MC task (log scale is used).

unit. The results are consistent with results in section 3.2.1 in that the closer we are to critical point the higher the AIS value. An interesting observation is that the OG scaling has a minimal AIS value as well as TE value among the scalings $\rho = 0.6$, $\rho = 0.95$, OG and ON.

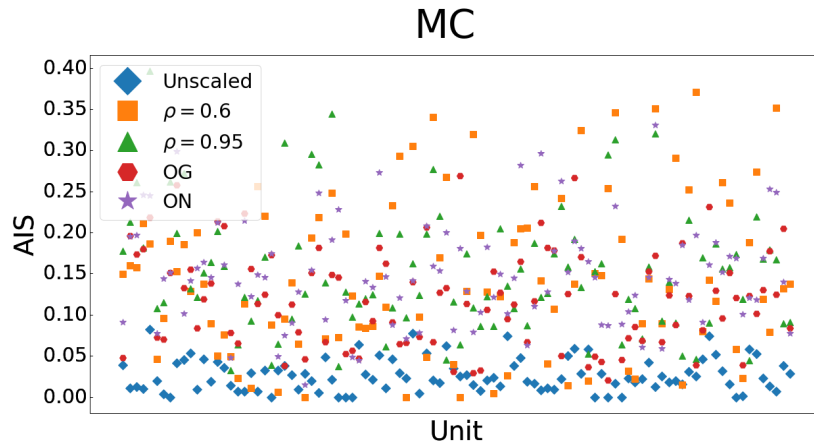


Figure 3.15: AIS values for every unit (N) in various reservoir scalings in MC task.

We also looked at distributions of reservoir activation signals (figure 3.16) for different scalings. The values of all the scalings settings except for unscaled case are within the range where the activation function can be approximated by a linear function what means that the reservoir does not benefit from the nonlinearities of tanh activation function.

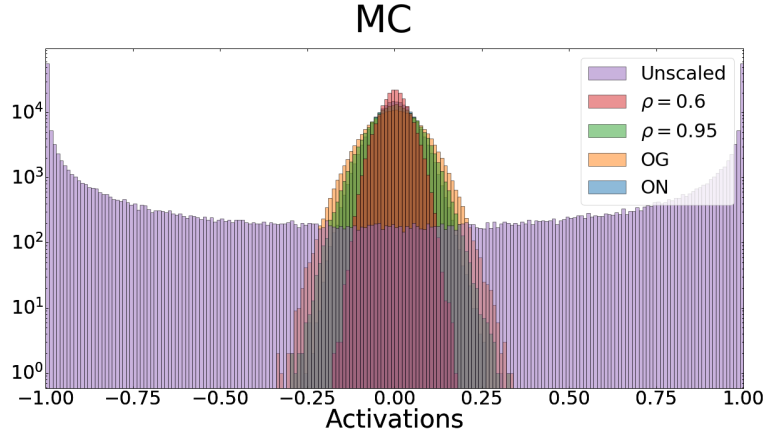


Figure 3.16: Reservoir neuron activation distributions for various reservoir scalings in MC task (in log scale).

MC task	Unscaled	$\rho = 0.6$	$\rho = 0.95$	OG	ON
MC	0.06	17.8	32.8	47.4	33.3
Average TE	0.007	0.091	0.047	0.041	0.061
Average AIS	0.027	0.146	0.151	0.12	0.148
Rel. entr. of TE	0.981	0.629	1.147	1.044	1.009
LE	0.53	-0.52	-0.06	-0.09	-0.16

Table 3.4: Quantitative measures for MC task, in case of initialized, scaled and orthogonalized reservoirs.

3.4.2 NARMA task

The results in NARMA task are very similar to the results in MC task. There is a visible change in the structure of TE matrices (Figure 3.17) with the transition from the unscaled to scaled cases. Also we can observe similar high TE target units (dark columns) for $\rho = 0.6$ and for $\rho = 0.95$, OG and ON cases and more spread distribution of TE in the reservoir. The Lyapunov exponent λ in all scalings is almost identical to the MC task.

The probability distribution of TE in the reservoir presented in Figure 3.17 look similar to the MC task as well. The biggest differences are between unscaled, scaled to $\rho = 0.95$, OG and ON, and $\rho = 0.6$ scalings. These differences are supported by the statistical testing we performed on the mean square errors (MSE) in every scaling using Kruskal–Wallis test. The differences in MSEs in the scalings $\rho = 0.95$, OG and ON are not statistically significant. Nevertheless from table ?? we get the same observation as

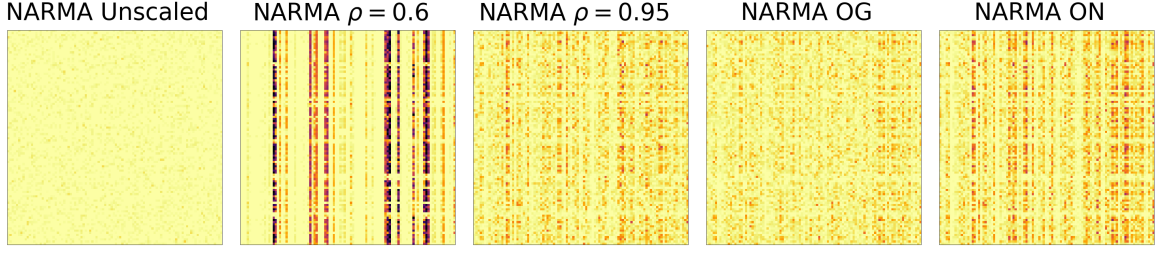


Figure 3.17: The matrices ($N \times N$) of TE values in the reservoir for different scalings in NARMA task. Rows of the matrix denote source units and columns denote target units. Dark color represents high values, light color represents low values.

in the MC task. In case of OG scaling the the performance is maximal, TE is minimal and relative entropy of TE is maximal among the scalings $\rho = 0.6$, $\rho = 0.95$, OG and ON.

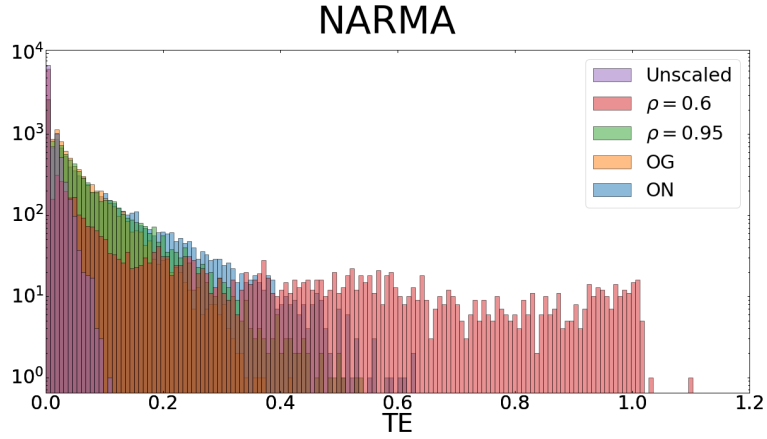


Figure 3.18: Histograms of TE distribution changes due to reservoir scaling in NARMA task (log scale is used).

The values of AIS for every unit in reservoir for every tested scaling shown in Figure 3.19, shows again qualitative similarities of MC and NARMA tasks. There are visible changes when comparing unscaled and scaled cases. In this case the lowest mean value of AIS among the scalings $\rho = 0.6$, $\rho = 0.95$, OG and ON is observed in case of $\rho = 0.95$.

Concerning the distribution of reservoir unit activations (Figure 3.20), it is even more focused when compared to the MC task. This means that the reservoir does not benefit from the nonlinearities of the tanh activation function for the scalings $\rho = 0.6$, $\rho = 0.95$, OG and ON, and could be replaced by a linear function.

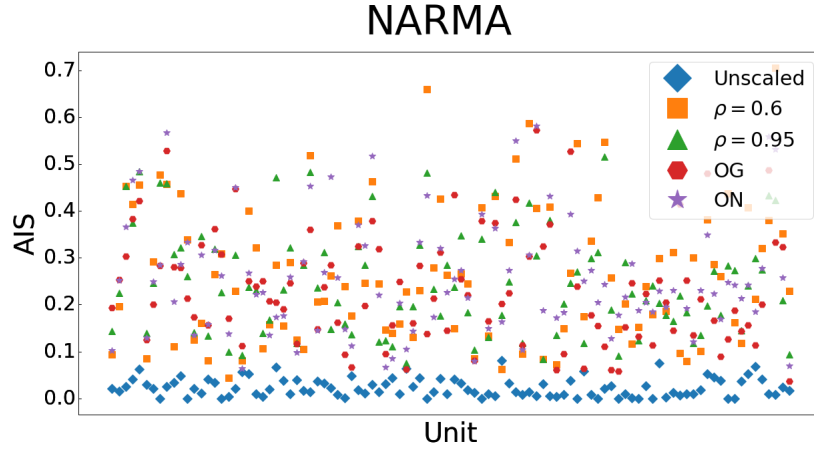


Figure 3.19: AIS values for every unit (N) in various reservoir scalings in NARMA task.

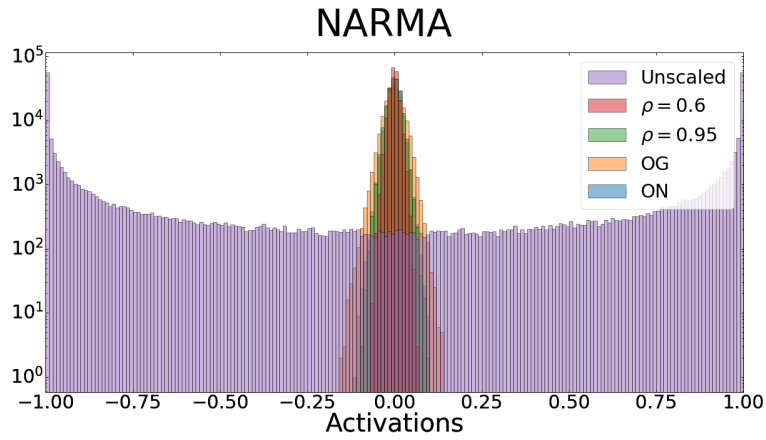


Figure 3.20: Reservoir neuron activation distributions for various reservoir scalings in NARMA task (in log scale).

NARMA	Unscaled	$\rho = 0.6$	$\rho = 0.95$	OG	ON
NRMSE	2.143	0.98	0.83	0.82	0.84
Average TE	0.007	0.087	0.052	0.043	0.066
Average AIS	0.023	0.267	0.247	0.232	0.257
Rel. entr. of TE	1.086	0.783	1.174	1.115	1.039
LE	0.52	-0.53	-0.062	-0.089	-0.16

Table 3.5: Quantitative measures for NARMA task, in case of initialized, scaled and orthogonalized reservoirs.

3.4.3 M–G task

In the case of M–G task there are noticeable differences in quality and quantity with the transition from scaled to unscaled when compared to the previous tasks. This

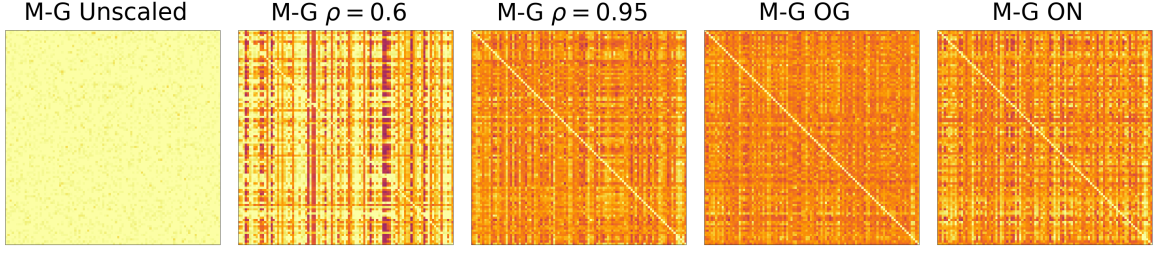


Figure 3.21: The matrices ($N \times N$) of TE values in the reservoir for different scalings in M–G task. Rows of the matrix denote source units and columns denote target units.

supports our findings from sections 3.2 and 3.3. There is only negligible global value of TE in the unscaled reservoir, but the minimal value among scaled reservoirs is for $\rho = 0.6$ as opposed to OG in MC task and $\rho = 0.95$ in NARMA task. The same goes for performance. We observe the best performance for the scaling $\rho = 0.6$, which is in the stable region of the Lyapunov exponent spectrum. We have performed a Kruskal–Walis test for differences in MSE among 5 scalings and found statistically significant differences in unscaled, $\rho = 0.6$ and $\rho = 0.95$. For the scalings $\rho = 0.95$, OG, ON there is no significant difference.

The distribution of TE in various scalings (Figure 3.22) shows some interesting similarities and differences when compared to MC and NARMA tasks. The maximum values of TE are lower than in MC and NARMA tasks ($\max \text{TE} \approx 0.6$ vs. $\max \text{TE} \approx 1.1$ respectively) but the distributions of unscaled and $\rho = 0.6$ look visually similar to MC and NARMA cases. Also quantitatively, the relative entropy of TE (Table ??) how smaller values compared to MC and NARMA tasks, meaning that the distribution of TE is more closer to uniform distribution. This can be observed visually in the TE matrices (Figure 3.21). Similarly to previous tasks the scaling with the best performance ($\rho = 0.6$) has the lowest value of mean TE and lowest value of relative entropy among the scalings $\rho = 0.6$, $\rho = 0.95$, OG, ON.

The values of AIS for individual units in various scaling are presented in Figure 3.23. Similarly to previous tasks, there is a noticeable shift from unscaled to scaled reservoirs but in M–G task the values of AIS are much higher ($\max \text{AIS} \approx 3.4$) than in MC and NARMA tasks ($\max \text{AIS} \approx 0.4$ and $\max \text{AIS} \approx 0.7$). The best performing scaling ($\rho = 0.6$) has the highest mean value of AIS among the scalings $\rho = 0.6, \rho = 0.95, \text{OG}$ and ON. This observation extends our findings from section 3.2. Compared to the MC and NARMA tasks, the best performing scaling had the lowest AIS among scaled

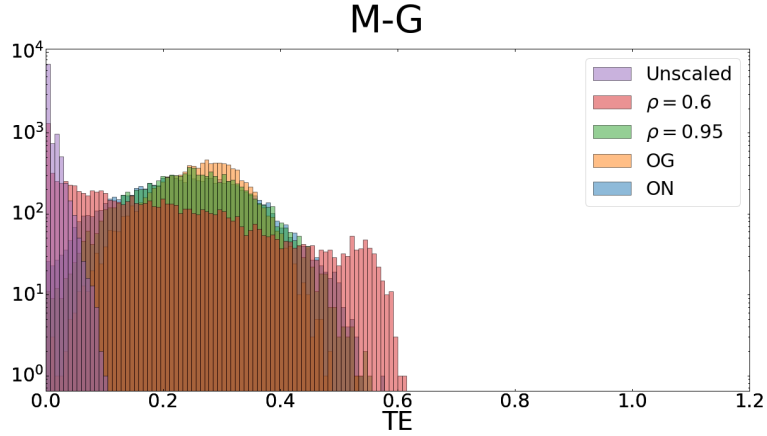


Figure 3.22: Histograms of TE distribution changes due to reservoir scalings in M–G task (log scale is used).

instances.

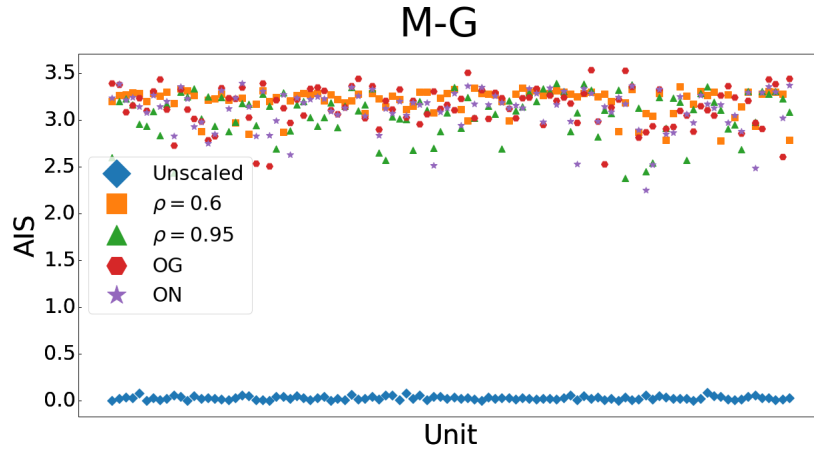


Figure 3.23: AIS values for every unit (N) in various reservoir scalings in M–G task.

The reservoir activations are similarly distributed as in previous cases (Figure 3.24). That is the activations in scaled reservoirs are very focused around zero meaning they operate in the linear mode and do not benefit from the nonlinearities of tanh activation function.

3.4.4 Lorenz task

The results in the Lorenz task confirm our findings in section 3.3 that there are two complexity classes in tested tasks. MC and NARMA, and M–G and Lorenz. The result regarding quantitative and qualitative properties of TE in Lorenz task are very much like the results in M–G task. The structure of TE matrices for various scalings

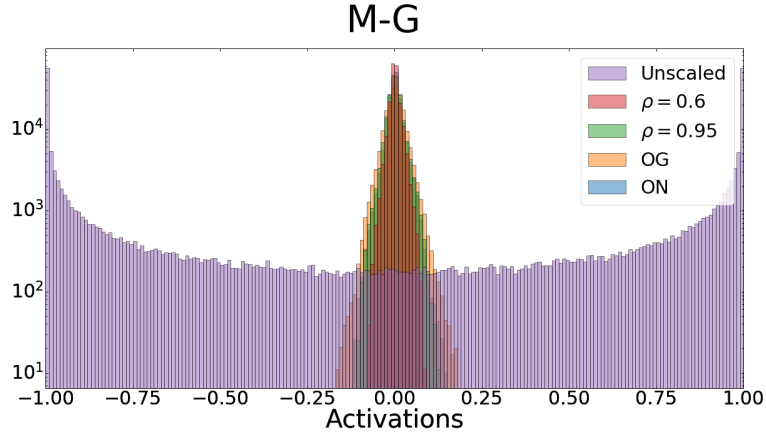


Figure 3.24: Reservoir neuron activation distributions for various reservoir scalings in M–G task (in log scale).

Mackey–Glass	Unscaled	$\rho = 0.6$	$\rho = 0.95$	OG	ON
NRMSE	1.13	0.00025	0.00026	0.0003	0.00026
Average TE	0.007	0.154	0.248	0.263	0.239
Average AIS	0.029	3.204	3.073	3.142	3.115
Rel. entr. of TE	1	0.266	0.386	0.587	0.318
LE	0.53	-0.52	-0.062	-0.09	-0.16

Table 3.6: Quantitative measures for M–G task, in case of initialized, scaled and orthogonalized reservoirs.

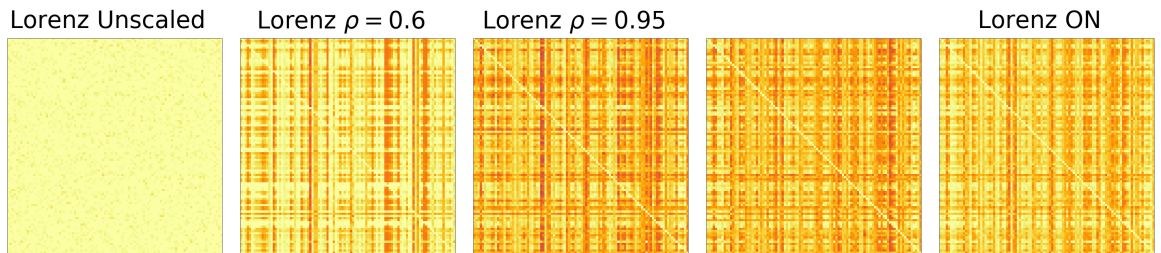


Figure 3.25: The matrices ($N \times N$) of TE values in the reservoir for different scalings in Lorenz task. Rows of the matrix denote source units and columns denote target units.

(Figure 3.25) resembles the TE matrices in M–G task, just with overall lower TE values. The best performance is observed in the $\rho = 0.6$ scaling just as in M–G task, which means better performance in stable regimes than closer to criticality. The Kruskal-Wallis test showed statistically significant differences between all scalings.

The distributions of various scalings in Lorenz task presented in Figure 3.25 show generally lower values of TE and also mean TE when compared to M–G task. Also the

structure of the distribution has some dissimilarities for scalings $\rho = 0.6$, $\rho = 0.95$, OG and ON. Regarding the relative entropy of TE shown in Table 3.7, in case of the scaling which has the largest performance ($\rho = 0.6$) has also the largest relative entropy of TE among the scalings $\rho = 0.6$, $\rho = 0.95$, OG and ON. This observation is a difference to NARMA and M-G prediction tasks where the scaling with the biggest performance has the smallest relative entropy of TE.

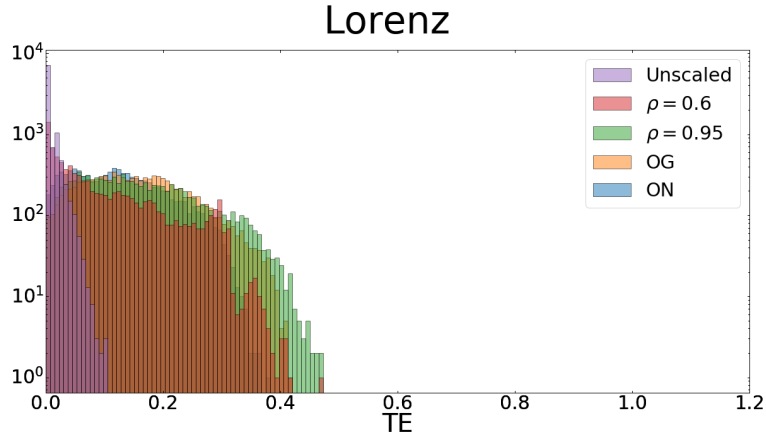


Figure 3.26: Histograms of TE distribution changes due to reservoir scaling in Lorenz task (log scale is used).

AIS global and individual unit values, shown in Figure 3.27, are again higher when compared to MC and NARMA tasks. Overall the plot is very similar to the case of M-G task and also the scaling with the best performance ($\rho = 0.6$) has the largest mean value of AIS among all scalings.

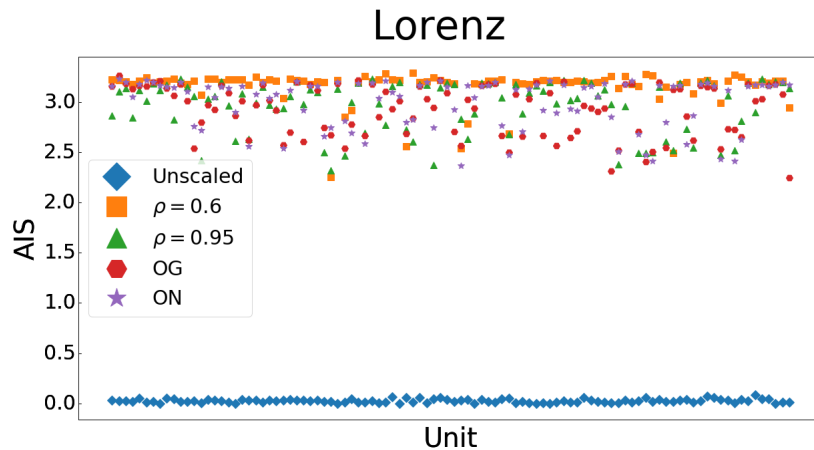


Figure 3.27: AIS values for every unit (N) in various reservoir scalings in Lorenz task.

The values of reservoir unit activations observed in Figure 3.28 for all scalings cover the whole range of the tanh activation function. This is a change when comparing to

Table 3.7: Quantitative measures for Lorenz task, in case of initialized, scaled and orthogonalized reservoirs.

Lorenz	Unscaled	$\rho = 0.6$	$\rho = 0.95$	OG	ON
NRMSE	0.54	0.00012	0.0013	0.0034	0.00097
Average TE	0.007	0.087	0.157	0.154	0.122
Average AIS	0.025	3.157	2.971	2.932	3.002
Rel. entr. of TE	1.018	0.642	0.231	0.19	0.217
LE	0.52	-0.74	-0.28	-0.35	-0.32

previous tasks. Still the most frequent activation values are around zero. This could be explained by the range of the driving signal and that we used the same input matrix \mathbf{w}^{in} which is not an optimal input matrix for the Lorenz task but a compromise for comparability reasons.

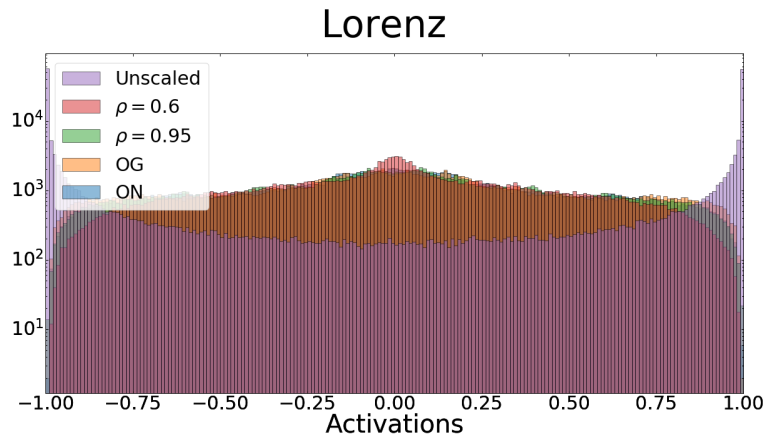


Figure 3.28: Reservoir neuron activation distributions for various reservoir scalings in Lorenz task (in log scale).

3.4.5 Conclusion

The results presented in this section confirm those in sections 3.2 and 3.3, that there are two complexity classes in relation to driving signals. This should come as no surprise since the driving signals in MC and NARMA tasks are stochastic, and in M-G and Lorenz are deterministic in nature. Performance wise M-G and Lorenz tasks do not benefit from criticality, as is the case of MC and NARMA tasks, but operate better in stable regimes.

When comparing task classes with complexity in mind, there is a general rise in performance, TE and AIS, and decline in relative entropy of TE in reservoir between NARMA and M–G/Lorenz tasks. On the other hand when comparing scalings within each task, the relationship is not so clear. In the stochastic complexity class (MC/NARMA) we observe rise of performance, and decline of TE and AIS. In the deterministic complexity class (M–G/Lorenz), rise in performance and AIS, decline in TE. These results support the findings in section 3.2 regarding the behavior of information measures in relation to stability in stable region. Additional information with regard to distribution of TE in the reservoir, shows that lower values of relative entropy of TE are accompanied with better performance when comparing scalings in MC, NARMA and M–G tasks. This is not the case in Lorenz task.

These results point to the hypothesis that there might be a relationship between performance, global TE and distribution of TE in the reservoir. More precisely that not only the amount of information transfer between units is important but also that it should be more uniformly distributed in the reservoir. These claims should be thoroughly investigated.

Chapter 4

Discussion

In this thesis we provided the basic theory of a specific RNN, namely the ESN model, and predictive causality measures grounded in information theory. We used this theory to examine information flow in the reservoir in relation to the stability of the network.

The experimental results presented in Section 3.2 partially confirm the results of Boedecker [4]. The information measures are maximized at the critical point in all examined tasks but in case of M-G and Lorenz prediction tasks stay high even in stable regimes. The performance in MC and NARMA tasks is maximized close to criticality similarly to [4] but the performance in our added deterministic driving signals, M-G and Lorenz, is maximized farther from the critical point in stable regimes. This indicates that the network makes use of the rich internal dynamics as well as slower fading memory associated with operating at the edge of chaos [11] in case of stochastic driving signal than deterministic driving signals.

Another interesting observation is the appearing relationship between TE and performance most noticeable in MC, NARMA and Lorenz tasks. It seems that high performance is associated with lower TE, and thus overall lower information exchange between units in the reservoir in the stable regime. The TE is generally higher in stable than in unstable regimes implying that also other factors are crucial for maximization of performance. It is necessary to rigorously test this observation to get a more precise answer to the question of the relationship between TE and performance. We leave this for further study.

Our exploration of optimal embedding vectors in Section 3.3 revealed that perhaps two "complexity" classes are present in the reservoir unit signals with respect

to tested tasks. Namely, stochastic (MC/NARMA) and deterministic (M-G/Lorenz). This finding supports the suggestion that in the stochastic class more complex dynamics are present and that the criticality is more important for better performance than in less challenging deterministic tasks.

When comparing between "complexity" classes in prediction tasks, the stochastic class, whose representative is the NARMA task, has generally lower performance, lower TE and lower AIS, and higher relative entropy of TE than the deterministic class. This indicates the possibility that besides global information flow in the reservoir the distribution of the information exchange is important in relation to maximizing performance. Maybe lower but more uniformly distributed would be better performance wise or dependent on task. Two examples of "complexity" classes are a small sample to make any conclusions. It would be interesting to find a representative task for every $k = 1, \dots, 6$ as we did in Section 3.3 for NARMA, M-G and Lorenz tasks, and examine TE, AIS, relative entropy, and performance in the same manner as done in Section 3.4. We leave this work for further study.

Bibliography

- [1] L. Barnett, A. B. Barrett, A. K. Seth, "Granger causality and transfer entropy are equivalent for Gaussian variables", *Physical Review Letters*, vol. 103, no. 23, pp. 238701, 2009.
- [2] J.M. Beggs, "The criticality hypothesis: how local cortical networks might optimize information processing", *Philosophical Transactions of the Royal Society A*, vol. 366, pp. 1864.
- [3] N. Bertschinger, T. Natschläger, "Real-time computation at the edge a of chaos in recurrent neural networks", *Neural Computation*, vol. 16, pp. 1413–1436, 2004.
- [4] J. Boedecker, O. Obst, J. Lizier, N. Mayer, M. Asada, "Information processing in echo state networks at the edge of chaos", *Theory in Biosciences*, vol. 131, pp. 205–213, 2012.
- [5] T. Bossomaier, L. Barnett, J. T. Lizier, *An Introduction to Transfer Entropy*, Springer, 2016.
- [6] M. Cencini, F. Cecconi, A. Vulpiani, *Chaos: From Simple models to complex systems (Series on Advances in Statistical Mechanics) (Volume 17)*, World Scientific Publishing Co, 2009.
- [7] P. Enel¹, E. Procyk¹, R. Quilodran¹, P. F. Dominey, "Reservoir computing properties of neural dynamics in prefrontal cortex.", *PLoS Computational Biology*, vol. 12, 2016.
- [8] I. Farkaš, R. Bosák, P. Gergeľ, "Computational analysis of memory capacity in echo state networks", *Neural Networks*, vol. 83, pp. 109–120, 2016.

- [9] J. Geweke, "Measurement of linear dependence and feedback between multiple time series", *Journal of American Statistical Association*, vol. 77, no. 378, pp. 304–313, 1982.
- [10] G. Gómez-Herrero, W. Wu, K. Rytanen, M. C. Soriano, G. Pipa, R. Vicente, "Assessing coupling dynamics from an ensemble of time series", *Entropy*, vol. 17, no.4, pp. 1958–1970.
- [11] S. Haykin, J. Principe, T. J. Sejnowski, J. McWhirter, Eds., *New Directions in Statistical Signal Processing: From Systems to Brain*, MIT Press, 2007.
- [12] S. Haykin, *Neural Networks and Learning Machines (3rd Edition)*, Prentice Hall, 2009.
- [13] K. Hornik, "Approximation capabilities of multilayer feedforward networks", *Neural networks*, vol. 4, pp. 251-257, 1991.
- [14] H. Jaeger, "The "echo state" approach to analysing and training recurrent neural networks", *German National Research Institute for Computer Science, Tech. Rep. GMD Report 148*, 2001.
- [15] H. Jaeger, "Short term memory in echo state networks", *German National Research Institute for Computer Science, Tech. Rep. GMD Report 152*, 2001.
- [16] E. T. Jaynes, *Probability Theory: The Logic of Science*, Cambridge University Press, 2003.
- [17] A. Kraskov, H. Stögbauer, P. Grassberger, "Estimating mutual information", *Physics Reviews E*, vol. 69, pp. 066138, 2004.
- [18] M. Lukoševičius, "A practical guide to applying echo state networks", In: G. Montavon, G. B. Orr, and K.-R. Müller (eds.) *Neural Networks: Tricks of the Trade*, 2nd ed. Springer, pp. 659-686, 2012.
- [19] D. MacKay, *Information Theory, Inference, and Learning Algorithms (fourth printing)*, Cambridge University Press, 2005.

- [20] M. Paluš, V. Komárek, Z. Hrnčíř, K. Šteřbová, "Synchronization as adjustment of information rates: Detection from bivariate time series", *Physical Review E*, vol. 63, pp. 046211, 2001.
- [21] M. Ragwitz, H. Kantz, "Markov models from data by simple nonlinear time series predictors in delay embedding spaces", *Physics Reviews E*, vol. 65, no. 5, p. 056201, 2002.
- [22] J. Schmidhuber, "Deep learning in neural networks: An overview", *Neural Networks*, vol. 61, pp. 85–117, 2015.
- [23] T. Schreiber, "Measuring information transfer", *Physical Review Letters*, vol. 85, no. 2, pp. 461–464, 2000.
- [24] C. E. Shannon, "A mathematical theory of communication", *Bell Systems Technical Journal*, vol. 27, pp. 379–423, 1948.
- [25] M. Wibral, R. Vicente, J. T. Lizier, Eds., *Directed Information Measures in Neuroscience*. Springer, 2014.

Appendix A

Used software

All experiments were done in **Python3.6** programming language, using *NumPy* library for basic numerical computations, *SciPy* library for the implementation of Digamma function computation, *scikit-learn* library for fast k -NN search implementing the k -d tree data structure, and *Matplotlib* library for graphics.